

Fabrication and Characterization of VO₂ Thin Films using Pulsed DC Magnetron Sputtering.

by

Juan Antonio Santiago Santos

Thesis submitted for the requirements for the degree of

MASTER OF SCIENCES

in

Physics

UNIVERSITY OF PUERTO RICO

MAYAGÜEZ CAMPUS

2015

Approved by:

Félix E. Fernández, PhD.
Graduate Committee President

Date

Pablo Marrero, PhD.
Graduate Committee Member

Date

Sergiy Lysenko, PhD.
Graduate Committee Member

Date

Rogelio Palomera, PhD.
Representative of Graduate Office

Date

Rafael Ramos, PhD.
Physics Department's Chairman

Date

I would like to dedicate this thesis to my whole family and Delva, for always believing in me...

Me gustaria dedicar esta tesis a toda mi familia y a Delva, por siempre creer en mi...

Declaration

I hereby declare that except where specific reference is made to the work of others, the contents of this dissertation are original and have not been submitted in whole or in part for consideration for any other degree or qualification in this, or any other University. This dissertation is the result of my own work and includes nothing which is the outcome of work done in collaboration, except where specifically indicated in the text. This dissertation contains less than 65,000 words including appendices, bibliography, footnotes, tables and equations and has less than 150 figures.

Juan Antonio Santiago Santos

2015

Acknowledgements

And I would like to acknowledge everyone who in some way or other collaborated with the realization of this work. Special thanks to Félix Fernández Ph.D. for accepting the challenge to guide me throughout these past few years. I would also like to thank Alfredo Moreu, who was an indispensable help and a good friend.

Abstract

Vanadium dioxide (VO_2) is one of the many oxide phases of vanadium, which exhibits a semiconducting monoclinic stable phase up to 68°C . At temperatures over $\sim 68^\circ\text{C}$ the stable phase for VO_2 is tetragonal and exhibits metallic conduction. Accompanying the abrupt and reversible phase change, the electrical resistivity and infrared transmittance changes substantially. Physical vapor deposition of VO_2 thin films is often performed successfully by Pulsed Laser Deposition (PLD), but this technique is not easily scaled up for large substrate areas. Sputtering can offer an alternate route which is easily scalable up to arbitrary size, but presents a challenge due to the technical difficulties that arise when depositing dielectric materials and, in the particular case of VO_2 requires very good control of film oxidation. Pulsed-DC reactive sputtering can solve the question of efficiently depositing uniform films of poorly conducting materials, but so far conditions have not been achieved to produce VO_2 films with electrical and optical response comparable to those obtained from PLD. The present work further investigated adequate parameters for VO_2 deposition via Pulsed-DC reactive sputtering. We were able to successfully deposit monoclinic VO_2 on glass at relatively low temperatures of $\sim 400^\circ\text{C}$ with a partial oxygen pressure of 0.5mTorr, but initial results were not easily reproducible, apparently because of the need to control the oxygen pressure very accurately. The results were improved by implementing post-deposition annealing methods. For measuring the electrical and optical changes of the films as a function of temperature, a software application was developed

using the LabVIEW platform. The software allowed for automatic data acquisition while the system took repeatable and accurate measurements. Electrical resistance characterization showed changes as high as three orders of magnitude with sharp hysteresis $\sim 11^\circ\text{C}$ wide. The optical transmittance in the infrared range also exhibited abrupt reductions of 36% during phase transition with similar hysteresis. Structural characterization by x-ray diffraction (XRD) showed that both, annealed and non-annealed samples exhibited the presence of monoclinic VO_2 with a high preference for alignment along the (100) plane. Estimates for grain size were also obtained from XRD and showed a slight reduction in grain size perpendicular to the (100) plane as the annealing time was increased. Further analysis was done on the samples with Atomic Force Microscopy techniques which revealed lateral grain sizes of 110 nm for samples annealed during 20 minutes and an increase to 300 nm for samples annealed for 45 minutes.

Resumen

El dióxido de vanadio (VO_2) es una de las varias fases de oxidación del vanadio, el cual exhibe una fase monoclinica semiconductor estable hasta 68°C . A temperaturas sobre $\sim 68^\circ\text{C}$ la fase estable para VO_2 es tetragonal y exhibe conducción metálica. Acompañando al cambio de fase abrupto y reversible, la resistividad y la transmitancia en el infrarojo cambian substancialmente. La deposición de películas delgadas de VO_2 por vapores generados físicamente se logra comúnmente de manera exitosa por Deposición por Láser Pulsado (PLD), pero esta técnica no se extiende fácilmente para sustratos con áreas grandes. El “sputtering” ofrece una alternativa viable que se puede aplicar a sustratos de escala arbitraria, pero representa retos debido a dificultades técnicas que surgen cuando se depositan materiales dieléctricos y, en el caso particular del VO_2 , requiere muy buen control de la oxidación de la película. El “sputtering” reactivo con alimentación DC-pulsada puede resolver el problema de la deposición uniforme de películas de materiales con baja conducción, pero hasta ahora no se han encontrado condiciones que logren producir películas de VO_2 con características eléctricas y ópticas que sean comparables con las obtenidas por DLP. El presente trabajo adelanta la investigación acerca de los parámetros adecuados para la deposición de VO_2 mediante sputtering reactivo con DC-Pulsado. Logramos de manera exitosa la deposición de VO_2 monoclinico sobre vidrio a temperaturas relativamente bajas de $\sim 400^\circ\text{C}$ usando una presión parcial de oxígeno de 0.5 mTorr, pero los resultados iniciales no fueron fácilmente reproducibles, aparentemente por la

necesidad de controlar de manera muy precisa la presión de oxígeno. Los resultados fueron mejorados mediante la implementación de métodos de recocido post-deposición. Para la medición de los cambios eléctricos y ópticos de las películas como función de la temperatura, se desarrolló un programado usando la plataforma LabVIEW. El programado permitió la adquisición automática de datos mientras el sistema tomaba medidas repetibles y precisas. La caracterización eléctrica mostró cambios tan grandes como 3 órdenes de magnitud con histéresis agudas y anchos de 11°C . La transmitancia óptica en el rango infrarrojo también exhibió reducciones abruptas de 36% durante la transición con histéresis similares. La caracterización hecha por difracción de rayos x (DRX) demostró que ambas películas, las recocidas y las no recocidas, mostraron la presencia de VO_2 monoclinico con una marcada preferencia a la alineación en el plano (100). Estimados sobre el tamaño del grano se obtuvieron de los resultados de DRX y mostraron una ligera reducción en el tamaño de grano cristalino en la dirección perpendicular al plano (100) según se aumentó el tiempo de recocido. Además, las muestras se estudiaron mediante técnicas de microscopía de fuerza atómica (MFA) las cuales revelaron tamaños laterales para los granos de 110 nm para las muestras recocidas por 20 minutos y un incremento hasta 300 nm para las muestras recocidas por 45 minutos.

Table of Contents

Table of Contents	ix
List of Figures	xi
List of Tables.....	xiii
Chapter 1 Introduction.....	1
1.1 Crystalline Structure of VO ₂	4
Chapter 2 Previous Work	9
2.1 Previous Work on Vanadium Oxides Deposition.....	9
Chapter 3 Experimental Procedure.....	18
3.1 Substrate preparation	18
3.2 Helium Cycle Cryogenic Vacuum Pump.....	20
3.2.1 Cryopump Regeneration	21
3.3 Deposition Chamber Vacuum.....	21
3.4 Temperature Control.....	23
3.4.1 Temperature controller adjustment.....	23
3.4.2 Substrate Heating	24
3.5 Deposition Ar/O ₂ Pressure.....	25
3.6 Sputtering Process.....	26
3.6.1 Plasma Magnetron Cathode	26
3.6.2 Pulsed DC Signal	27

3.6.3	Vanadium deposition	28
3.7	Sample Annealing	30
3.8	Sample Thickness	30
3.9	Vanadium Oxide Transition Testing.....	32
3.9.1	Optical Transition	33
3.9.2	Electrical Resistance	34
3.9.3	LabVIEW Software	34
Chapter 4	Results and Discussion	38
4.1	Deposition Parameters	40
4.2	Electrical Resistance and IR Transmittance Results.....	41
4.2.1	Effects of Deposition Temperature.....	41
4.2.2	Effects of Annealing	43
4.3	XRD Results	46
4.4	AFM Imaging.....	50
Chapter 5	Conclusion	53
References	56
Appendix A	Additional Data.....	A-1
A.1	Transmittance Laser Calibration	A-1
A.2	LabVIEW Measurement File	A-2

List of Figures

Figure 1.1 (a) Projection of rutile VO ₂ along [001] drawn white for vanadium atoms at $Z=0$ and grey for vanadium atoms at $Z=1/2$. (b) Projection along [010]. Vanadium atoms build chains parallel to the c axis of the structure. Vanadium atoms are drawn black and oxygen atoms white. Taken from [7].	5
Figure 1.2 A) VO ₂ (M) structure as projected along [100]. B) Previous c axis of the rutile cell projection along [010]. The double liaison V-O is drawn as a heavy line. The ex-rutile cell is drawn as a grey line in order to emphasize the distortion between VO ₂ (R) and VO ₂ (M). Taken from [7].	6
Figure 1.3 A) Structure of VO ₂ (B) as projected along the [010]. B) Structure of VO ₂ (M) as projected along the [001]. In both images the alternating layers of oxygen octahedrons are drawn white and grey respectively. Taken from [7].	7
Figure 2.1 A) Phases identified by x-ray diffraction in reactive sputtered vanadium oxide as a function of the deposition conditions. Black dots indicate conditions under which oxides, other than VO ₂ , were obtained. The black data points identify additional conditions under which the phase indicated was identified. B) Resistivity results for one of the samples produced by Kusano <i>et al.</i> . Both taken from [14].	13
Figure 2.2 A) XRD results for samples grown on glass substrate. B) Resistance as a function of temperature for sample grown on glass substrate. Both taken from [15].	14
Figure 2.3 Square Pulsed-DC signal supplied for the deposition process. The negative segment (τ_{on}) represents the deposition voltage potential while the (τ_{rev}) allows for charge accumulation discharge. Taken from [16].	16
Figure 2.4 Represented by black diamonds is the On-pulsed average power and deposition rate by circles, both as a function of the frequency. Taken from [16].	17
Figure 3.1 Parts identification and stages of cooling during cryopumping [17].	19
Figure 3.2 Residual gas analysis performed with a Spectra Instrument's Vacscan on the deposition chamber before deposition. Total pressure of the chamber was measured to be 1.1 μ Torr.	22

Figure 3.3 Honeywell UDC 2500 temperature controller adjustment graph. The substrate's temperature was obtained with an Omega HH-20A. Both instruments used a type-K thermocouple.....	24
Figure 3.4 A) Sputtering while the shutter was closed in order to clean substrate's surface. B) Vanadium deposition on glass substrate after 5 minutes of deposition, B) 10 minutes and C) 15 minutes.....	29
Figure 3.5 Profilometer graph for a vanadium deposition, as recorded by a Tencor Alpha-Step 100, using a 5000 Angstrom (5 kÅ) scale setting.....	31
Figure 3.6 Experimental setup for optical IR transmittance and electrical resistance testing of vanadium samples.....	32
Figure 3.7 LabVIEW software user interface (Front Panel).....	35
Figure 3.8 Temperature Calibration on MMR K20 temperature controller.....	36
Figure 4.1 A) Electrical resistance and B) Infrared transmittance of samples without annealing process. Arrows show direction of the heating cycle.....	42
Figure 4.2A) Electrical resistance and B) Infrared transmittance of samples grown under same conditions but subjected to different annealing times. Heating cycle follows same paths as in Figure 4.1.....	45
Figure 4.3 XRD results for VO ₂ samples.....	47
Figure 4.4 A) XRD comparison for not annealed and annealed sample. B) Electrical resistance testing for same samples.....	50
Figure 4.5 AFM images for A) VJS-038 and B) VJS-040. C) Surface profile of VJS-040 along the line shown to the right. D) Close up for AFM results of VJS-040. Images processed using WSxM [21].....	52

List of Tables

Table 1.1 Table of Densities for Vanadium Dioxide structures.	4
Table 4.1 Deposition parameter range.	38
Table 4.2 Deposition parameters for most relevant results. For all samples, the argon deposition pressure was kept at 5.0 mTorr.	40
Table 4.3 Electrical and optical characterization results for non-annealed samples.	43
Table 4.4 Electrical and optical characterization results for annealed samples. Shaded columns depict the change on the magnitude of the phase transitions.	44
Table 4.5 Grain size for annealed samples based on the XRD results.	49
Table 4.6 AFM Roughness results for annealed samples VJS-38 and 040.	50
Table 5.1 IR Transmittance characterization laser calibration.	A-1
Table 5.2 File created by the LabVIEW software. Column order: Temperature (K), IR transmittance (%) and Resistance (Ohm)	A-4

Chapter 1 Introduction

Vanadium dioxide (VO_2) is one of the many oxidation phases of vanadium, a transition metal whose partially filled d sub-shell gives it the capability to have diverse oxidation states (+2, +3, +4, +5). Specifically, VO_2 has been studied for the last half century [1] due to its fascinating electrical and optical characteristics which show a strong dependence on temperature near the material's phase transition between a monoclinic and a tetragonal structure, which occurs near 68°C (on heating). This structural change causes an increase in electrical conductivity and magnetic susceptibility of the bulk material [2]. In bulk crystals, the change in resistivity is of order up to $10^5\ \Omega\cdot\text{cm}$, with a hysteresis width of approximately 1°C . On the other hand, VO_2 thin films have a hysteresis width of at least a few degrees and up to 10°C to 15°C , with lower changes in the resistivity values.

The optical properties of VO_2 are also affected during this transition, especially on the $0.8\text{-}2.2\ \mu\text{m}$ near infrared region. Heating a thin film of VO_2 (with a thickness between $1.8\ \text{k}\text{\AA}$ to $4.5\ \text{k}\text{\AA}$), causes the IR transmittance of the material to drop from $\sim 20\%$ to 1.0% transmission, while showing a hysteresis width of $\sim 5^\circ\text{C}$. Of course, transmittance values are highly dependent on the sample thickness, but the change, over just a few degrees of temperature is remarkable. This material has also generated interest due to the fact that the insulator-metal transition (IMT)

can be induced by ultrashort laser pulses [3] [4]. During the transition some characteristics of the material are affected differently if the material is nanostructured [5].

There are various methods for creating VO₂ thin films which include Chemical Vapor Deposition (CVD), Sol-Gel synthesis, sputter deposition and Pulsed Laser Deposition (PLD) [2]. Out of these methods the most common one employed for VO₂ thin film deposition has been PLD, which is very well suited for growing oxide thin films. Closely followed in popularity for growing VO₂ thin films is reactive sputtering. The first records for VO₂ deposition via reactive sputtering are dated back to 1967 [6].

For our work we chose to work with pulsed-DC magnetron sputtering. Sputtering offers some advantages when compared to PLD, some of which include better film thickness uniformity and efficiency during the deposition process [2]. Because of this, sputtering processes can be easily scaled to larger substrates. This offers the possibility to easily scale our results to manufacturing applications.

Sputtering works by creating a high voltage between electrodes of a sputtering gun, which is inside a vacuum chamber filled with a gas (the “working gas”) at a pressure of order 1 to 10 mTorr. The potential causes the gas, in most cases argon, to become ionized. Argon ions within the weak plasma which is formed are now accelerated towards the negative electrode (the cathode) of the gun. The target of the material one desires to deposit, which we assume for the moment is a metal, is directly attached to the cathode electrode, so it is bombarded by the

accelerated gas ions, which acquire high kinetic energies after traversing the potential difference. Momentum transfer by these ions causes atoms from the target's surface to be released, that is, "sputtered" with relatively large kinetic energies. That is, sputtered atoms have kinetic energies which are larger than the average energies of atoms evaporated from a melt of the same target material. Atoms now travel through the plasma and get deposited on any directly exposed surfaces, including the substrates. If the working gas included a reactive gas, such as oxygen, reactions can occur as the film is being deposited. This arrangement is called "reactive sputtering", and is of interest when depositing oxide thin films. However, oxygen will react also with the target, causing it to become rapidly coated with the oxide and, if the oxide is dielectric, impairing or even stopping the sputtering process. Since vanadium oxides are in general poor conductors, the use of reactive sputtering is not efficient. Deposition of dielectric materials is usually accompanied by strong arcing problems caused by oversaturation of charges on the target's surface. To reduce this effect RF (radio frequency) sputtering or Pulsed-DC sputtering is usually the preferred method. During RF Sputtering the potential applied to the target varies from a high positive voltage to a minimum negative voltage at a given frequency as a sinewave. The positive voltage allows for the target's surface to be discharged, while the deposition occurs during the negative part of the cycle. The downside to this method is that the effective deposition time is reduced to less than half when compared to DC reactive sputtering, making the process highly inefficient.

Pulsed-DC sputtering produces a voltage in the form of an asymmetric square wave. This allows us to control the discharge time and deposition time as well as the voltage for discharging and deposition as separated parameters. By implementing Pulsed-DC the target can be safely discharged preventing excessive arcing without severely affecting the deposition time. A more detailed explanation of this technique is given in section 2.1.

1.1 Crystalline Structure of VO₂

There are four main polymorphic structures of vanadium dioxide: VO₂(R), VO₂(M), VO₂(B) and VO₂(A). All of these are based on a, more or less regular, body centered tetragonal lattice (bct), with oxygen atoms forming octahedrons while the vanadium atoms occupy the centers (octahedral sites) and are located at the lattice points of the bct lattice. These structures are usually divided into two groups depending on the orientation of the fourfold axis of the oxygen octahedral. This variation on the orientation of the octahedrons also implies a different cell size which can be noted by the difference of densities between the structures shown in Table 1.1 below.

Structure	VO ₂ (R)	VO ₂ (M)	VO ₂ (B)	VO ₂ (A)
Density (g/cm ³)	4.67	4.67	4.031	4.035

Table 1.1 Table of Densities for Vanadium Dioxide structures.

In the case of rutile-type VO₂(R) and monoclinic VO₂(M), the oxygen octahedral axes are aligned along two perpendicular directions, in contrast with VO₂(B) and VO₂(A) where the axis is mainly aligned along a single direction.

Of these four main structures, VO₂(R) is considered to be the most stable of them all, that being on a temperature range from 68°C to 1540°C. Within this temperature range rutile-type vanadium presents a tetragonal structure with parameters $a=b=4.55\text{Å}$, $c=2.88\text{Å}$ and $Z=2$. This structure belongs to the crystallographic group P4₂/mmm (group 77). At the center of each regular oxygen octahedron lies a vanadium atom forming two V-O bonds at 0.1933nm and the other four bonds at 0.1922nm . For these two structures the fourfold axes of the octahedrons are aligned in an alternating fashion the ab plane as shown in Figure 1.1 [7].

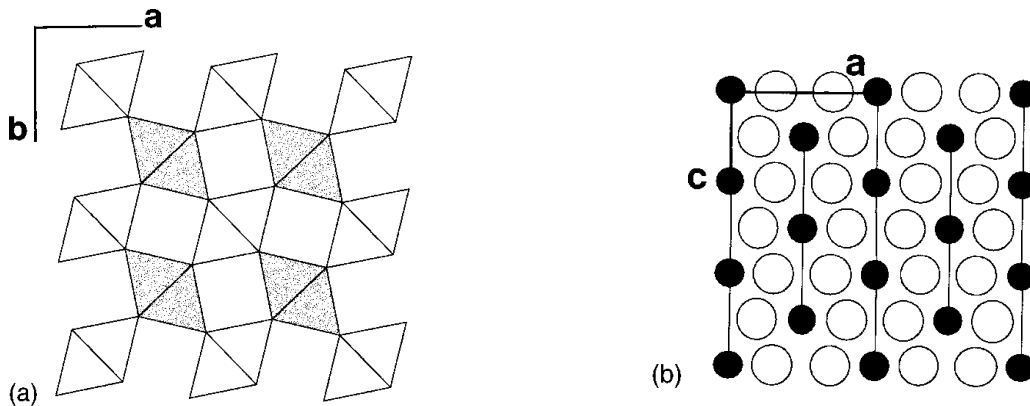


Figure 1.1 (a) Projection of rutile VO₂ along [001] drawn white for vanadium atoms at $Z=0$ and grey for vanadium atoms at $Z=1/2$. (b) Projection along [010]. Vanadium atoms build chains parallel to the c axis of the structure. Vanadium atoms are drawn black and oxygen atoms white. Taken from [7].

Heating a VO₂ sample past 68°C induces the formation of monoclinic VO₂(M) due to pairing and sideways shifting of pairs of V⁴⁺ ions along the C_R axis. This pairing causes the previous rutile cell symmetry of VO₂ to drop, obtaining new monoclinic cell parameters of $a=5.75 \text{ \AA}$, $b=5.42 \text{ \AA}$, $c=5.38 \text{ \AA}$, $\beta=122.6^\circ$ and $Z=4$ [7]. This time the new monoclinic structure is grouped in the P2₁/c (14) space group. The shifting also causes some of the V-O distances to shorten (0.176 nm) which corresponds to a double link. Between the vanadium atoms there are now two different distances, 0.2615 nm and 0.3162 nm, in contrast to the rutile structure where all vanadium atoms were spaced at 0.2851 nm along the c_R direction.

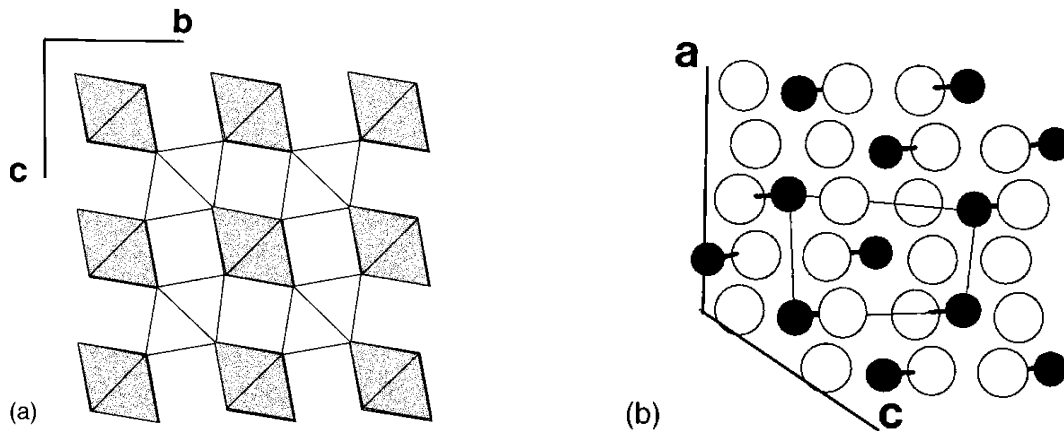
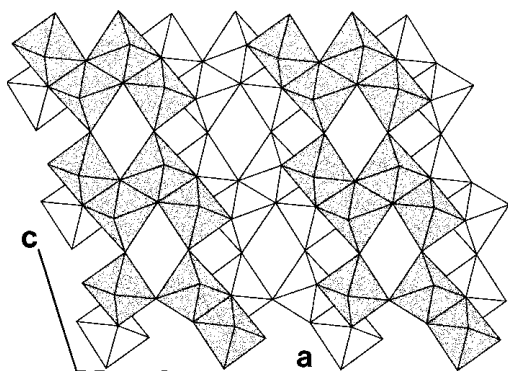


Figure 1.2 A) VO₂(M) structure as projected along [100]. B) Previous c axis of the rutile cell projection along [010]. The double liaison V-O is drawn as a heavy line. The ex-rutile cell is drawn as a grey line in order to emphasize the distortion between VO₂(R) and VO₂(M). Taken from [7].

The remaining two structures are a far step from the rutile structure already discussed, showing larger cell sizes and octahedrons aligned mostly in one crystallographic direction. VO₂(B) is a monoclinic structure that was first reported by Théobald [8]. He reported that

VO₂(B) could be obtained by reduction of V₂O₅ via hydro-thermal treatment. This new structure showed cell parameters $a = 512.03 \text{ \AA}$, $b = 53.693 \text{ \AA}$, $c = 56.42 \text{ \AA}$ and $\beta = 106.6^\circ$, $Z=8$ and is classified under the monoclinic space group C2/m [7]. Figure 1.3 A) shows the structure of VO₂(B) along the (010) plane. From this figure we can see that the structure of VO₂(B) is made up of two of the same octahedral layers, the second one being shifted by $(\frac{1}{2} \frac{1}{2} 0)$. Also, it can be noted that the oxygen octahedrons are somewhat deformed because the vanadium atoms no longer are located at the center, though not all of them are deformed in the same direction as shown in Figure 1.3 A. Therefore this structure has two different oxygen octahedrons whose fourfold axes align in more or less the same crystallographic direction.

A)



B)

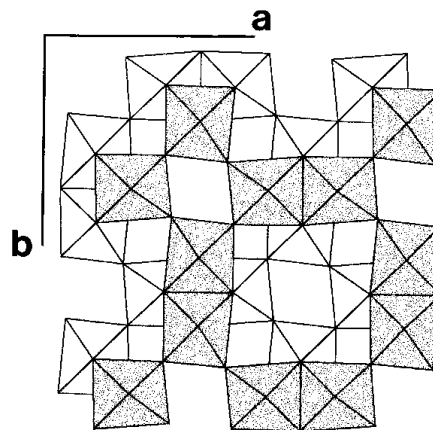


Figure 1.3 A) Structure of VO₂(B) as projected along the [010]. B) Structure of VO₂(M) as projected along the [001]. In both images the alternating layers of oxygen octahedrons are drawn white and grey respectively. Taken from [7].

The last of the metastable phases of vanadium dioxide to discuss is VO₂(A). This structure was also reported by Theobald who described it as a transition phase from VO₂(B) to VO₂(R). According to Oka *et al.* [9], VO₂(A) has a tetragonal structure with cell parameters $a = b = 8.44 \text{ \AA}$, $c = 7.68 \text{ \AA}$ and $Z = 16$ and belongs to the P42/nmc (138) space group. Figure 1.3 B) shows the structure of VO₂(A) as projected along the direction of [001]. Just as in VO₂(B), we can see that the fourfold axes of the oxygen octahedra are aligned in one direction, this time the c axis. Since the structure is not as deformed as VO₂(B) there is just one type of octahedron.

Chapter 2 Previous Work

2.1 Previous Work on Vanadium Oxides Deposition

One of the earliest works done on VO_2 was published by F.J. Morin in 1959 [10]. Morin recalls that he had previously reported that lower titanium and vanadium oxides would behave like metals given the right conditions. It was then suggested that this was explained because in oxides at the beginning of the $3d$ series, the nonbonding (t_{2g}) orbitals extend out far enough causing an overlapping which in turns forms a narrow conduction band [11]. On his second paper on metal oxides, he reported to have found metal-to-insulator transitional behavior for various oxides, amongst them VO_2 . On this latter work, the VO_2 samples showed the conductivity changing by two orders of magnitude with a transition temperature that ranged from 335 K to 350 K for the heating cycle and 340 to 325 K for the cooling cycle [10]. It is worth noting that the samples produced by Morin were around 0.1mm in size, so Morin himself stated that the samples were too small for the four-point resistivity measurement and that the absolute value of conductivity quoted was somewhat in doubt due to contact resistance and dimensional uncertainty [10].

After Morin's publication other researchers dug deeper into understanding the VO₂ semiconductor to metal transition. A.S. Barker *et al.*, reported in 1965 on the changes of the optical properties of VO₂ thin films above and below their transition temperature [12]. Later on, in collaboration with Verleur, Barker determined the optical constants for VO₂ between 0.25 and 5 eV both below and above the semiconductor-metal transition temperature $T_i=340$ K [13]. Their measurements were based on reflectivity and transmission spectra and were measured on both single crystals and thin films. Below T_i there were four prominent absorption peaks found to be centered near photon energies of 0.85, 1.3, 2.8, and 3.6 eV. Above T_i , metallic free-carrier absorption was observed below 2.0 eV, but the same two absorption peaks near 3 and 4 eV were found to be present [13]. Verleur and Barker related the energy location and polarization dependence of these two higher energy peaks to those found in rutile, and therefore interpreted them using the rutile band structure. Their results were consistent with a picture in which filled bands arising primarily from oxygen $2p$ orbitals are separated by approximately 2.5 eV from partially filled bands arising primarily from vanadium $3d$ orbitals. These results agreed with what was previously reported by Morin. On the high-temperature metallic phase, they found evidence for the overlapping of $3d$ bands such that at least two bands are partially occupied by the extra d electron per vanadium ion. On the low-temperature semiconductor phase, Verleur and Barker reported a band gap of approximately 0.6 eV within the $3d$ bands [13]. This gap separated two filled bands from higher-lying empty bands.

In 1968 G.A. Rozgonyi and D.H. Hensler published their work on VO₂ thin film deposition via reactive radio frequency (RF) sputtering. The thin films were deposited on glass, rutile, sapphire, and glazed ceramic. The deposition was performed in an argon and oxygen atmosphere where the ratio of gases was kept at a 100-1. As for the deposition itself, a metallic vanadium target was used and the power supply for the RF process was kept at 4.5 kV. The substrates were placed fairly close to the target at a distance 2.5" (63.5 mm) and kept at 400 °C during deposition. With a total gas pressure of 25 mTorr, the reported deposition rate was 15 Å/min. All the samples were grown to a final thickness of 600 Å. After deposition, all the samples were tested for conductivity and were examined using XRD. The samples grown on glass, sapphire and glazed ceramic showed a T_t of 68 °C while the samples grown on rutile showed a 10 °C lower T_t . The conductivity of the samples also varied according to the substrate used. The samples grown on glass and glazed ceramic reflected a conductivity value that ranged between 0.35 - 0.27 ($\Omega \cdot \text{cm}$)⁻¹ while the sapphire and rutile samples presented a conductivity range between 0.28 to 1.1x10² ($\Omega \cdot \text{cm}$)⁻¹ [13]. The XRD and electron microscopy test showed that the structure of the films also varied according to the substrate. A polycrystalline VO₂ structure with multiple grain sizes was found on the samples deposited over glass and ceramic while those on the other substrates had a more uniform and smooth structure. Based on their findings Rozgonyi *et al.* concluded that the substrate used has a vast influence on the electrical and structural properties of the VO₂ film.

In 1987 by Kusano *et al.* published their work on vanadium oxides deposition via reactive sputtering [14]. For their work, these authors used a 12.7cm diameter, 99.99% pure vanadium target which was operated at a 2.0 A discharge current level. A 10^{-6} Torr base pressure (p_b) was achieved before the deposition and an argon/oxygen mix was used as the working gas. The argon (99.99%) and oxygen (99.99%) were injected into the chamber via electronic mass flow controllers while the vacuum pump rate was held at 230 lt/min, all together to produce a deposition pressure (p_d) of 2.0 mTorr. The substrates used were borosilicate glass plates that were heated on a range between 300 to 500°C. Deposition rates with values 10 to 30 nm/min were achieved, while the final sample thickness ranged from 400 to 700 nm. On their work Kusano *et al.* were able to identify four main regions on which a given oxygen injection rate, constant discharge current and argon pressure would produce different deposition rates. Changes in the partial oxygen pressures (p_{O_2}) lower than 0.3 mTorr would not cause major changes on the sputtering rates. Pressures on the 0.3 to 0.5 mTorr range would cause an increment on the discharge voltage as well as a noticeable reduction on the deposition rate. Higher oxygen pressures in the range of 0.5 to 0.7 mTorr would cause even further increment on the discharge voltages and, as before, even further reduction of the deposition rate. In this pressure range Kusano *et al.* reported that the deposition process was starting to suffer instability due to the charge accumulation on the surface of the vanadium target. Oxygen pressures above 0.7 mTorr caused over accumulation of charge, or as is often referred to, "poisoning", of the target surface, decreasing the vanadium sputtered flux [14].

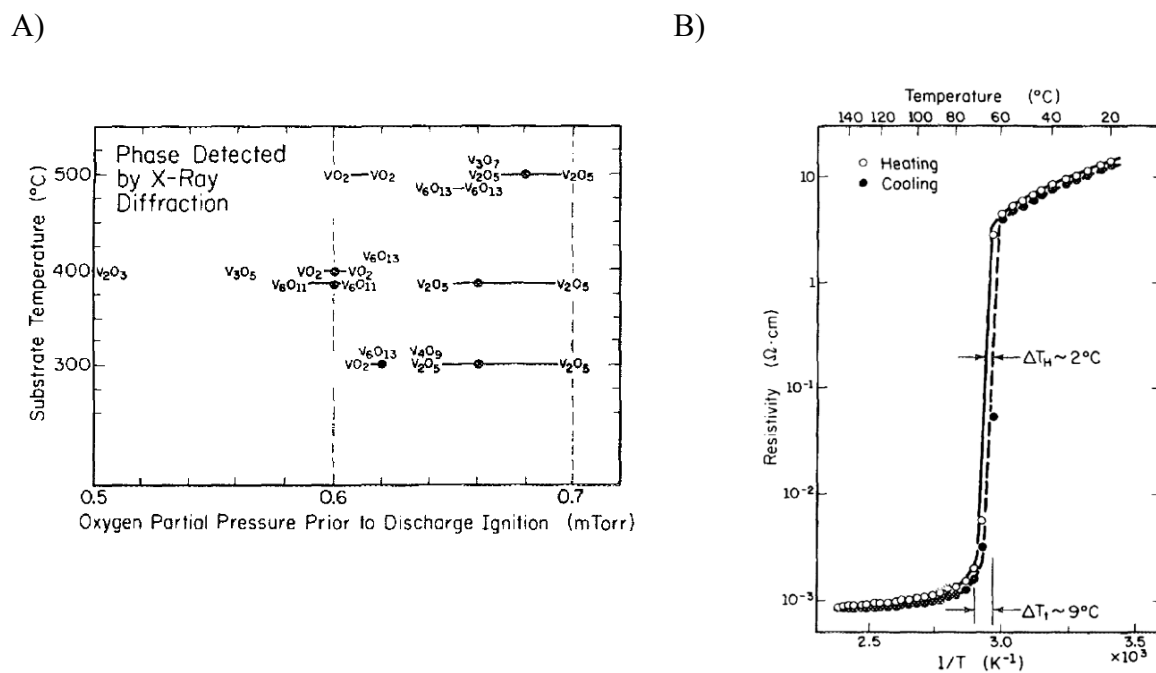


Figure 2.1 A) Phases identified by x-ray diffraction in reactive sputtered vanadium oxide as a function of the deposition conditions. Black dots indicate conditions under which oxides, other than VO_2 , were obtained. The black data points identify additional conditions under which the phase indicated was identified. B) Resistivity results for one of the samples produced by Kusano *et al.*. Both taken from [14].

In their work, Kusano *et al.* concluded that a substrate temperature of around $500^{\circ}C$ or less must be used for VO_2 deposition onto glass substrates or onto multilayer structures. They also noted that microstructure variations along with the nonlinearities of the reactive sputtering process limit the range of partial oxygen pressures that can be used for the process. Furthermore, they found evidence that an optimum combination of deposition and annealing conditions could yield even higher resistivity ratios at substrate temperatures not exceeding $400^{\circ}C$.

More recently W.J. Torné deposited vanadium oxides using pulsed DC sputtering technique. Torné grew thin films of vanadium dioxide on glass and sapphire substrates, analyzed the crystal structure of the samples by x-ray diffraction (XRD) and characterized their electrical properties by measuring resistance via the two-contact method, as a function of temperature, in the range from room temperature to 90°C or more.

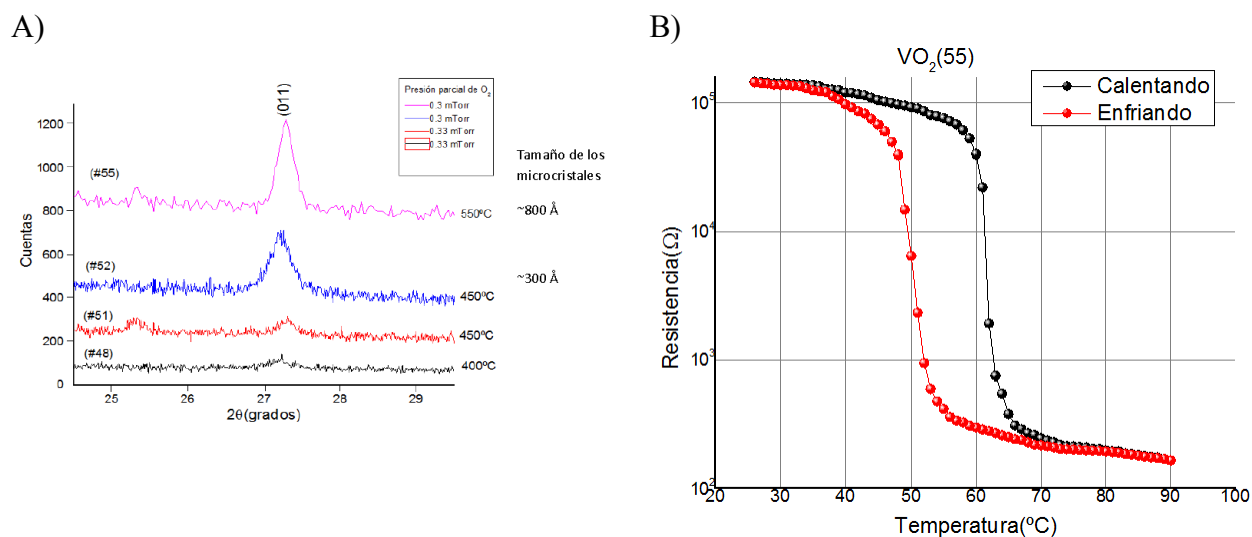


Figure 2.2 A) XRD results for samples grown on glass substrate. B) Resistance as a function of temperature for sample grown on glass substrate. Both taken from [15]

Torné was able to deposit monoclinic VO₂ phase films using a 90 sccm argon flux at a total sputtering pressure of 6.03 mTorr while the oxygen partial pressure was measured at ~ 0.33 mTorr. The sputtering cathode was held at a constant power of 300 W and the parameters for the pulsed DC signal used were 150 kHz frequency with an inverse time of 2.5 μsec . During sputtering the substrate was heated to a temperature of 550 $^{\circ}\text{C}$ [15]. After characterization Torné

reported that films grown on sapphire exhibited better crystal quality and their resistance change during the transition was greater than three orders of magnitude, with a narrow (3 °C) hysteresis curve, while those grown on glass exhibited a resistance change of over two orders of magnitude and a broad (12 °C) hysteresis curve (see Figure 2.2 B). Although this work showed adequate conditions for VO₂ deposition, the range of possible fabrication parameters explored was somewhat limited. This allows us to further improve on the technique and obtain better results. Another limitation to the previous work was the fact that the only characterization made was electrical resistance as a function of temperature.

Belkind *et al.* considered pulsing parameter effects on thin film deposition during Pulsed-DC reactive sputtering [16]. These authors explain that using a DC signal alone while depositing dielectrics via reactive sputtering is usually accompanied by strong electrical arcing discharges. This arcing is mainly concentrated on a portion of the target surface that is not being strongly bombarded by the positive ions of the sputtering gas used during deposition. This lack of bombardment creates a dielectric layer on the surface of the target which accumulates positive charges that eventually cause arcing. Excessive arcing creates technical problems such as power supply failures and target surface scarring which may eventually cause even more arcing due to the creation of hotspots along scars and scratches on the surface of the target.

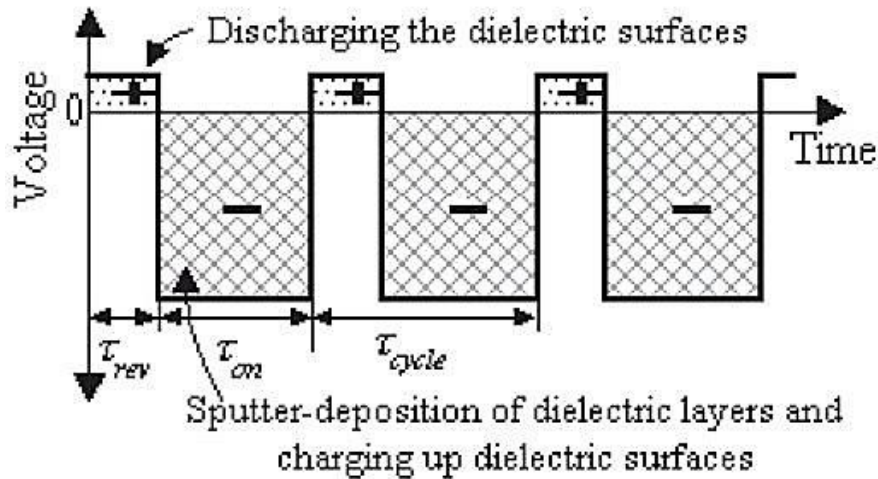


Figure 2.3 Square Pulsed-DC signal supplied for the deposition process. The negative segment (τ_{on}) represents the deposition voltage potential while the (τ_{rev}) allows for charge accumulation discharge. Taken from [16]

For their work, the Pulsed-DC signal, like the example shown on Figure 2.3, was generated using an Advance Energy Systems PinnaclePlus® Pulsed-DC power supply which was operated at constant power and current modes. The actual voltage and currents wave forms were recorded using a TDS 340 oscilloscope. During their work, Belkind *et al.* found that a minimum frequency f_{cr} must be used in order to completely discharge the target's surface from unwanted charge. They also noted that there is a minimum “time off value” $\tau_{off,min}$ necessary to avoid charge accumulations that causes smaller discharges or microarcs over extended periods of deposition. The values for $\tau_{off,min}$ necessary to avoid microarcs are mostly determined experimentally [16].

Belkind *et al.* were able to determine that the successful conditions for the deposition of aluminum oxides films. To avoid arcing, τ_{on} was kept no larger than 0.1 to 1 ms and the pulsating frequencies were far larger (100 to 350 KHz) than the critical frequencies which ranged from 1 to 10 KHz [16]. In this work it was concluded that dielectric materials can be effectively deposited while avoiding arcing and the technical problems associated with it. A minimum frequency f_{cr} or higher must be used as well as a minimum duty cycle. Increasing the frequency of the pulse presented a power loss which results in an apparent decreased in the deposition rate as shown in Figure 2.4 below. This can be easily explained since excessive switching will decrease the τ_{on} during which deposition is actually taking place.

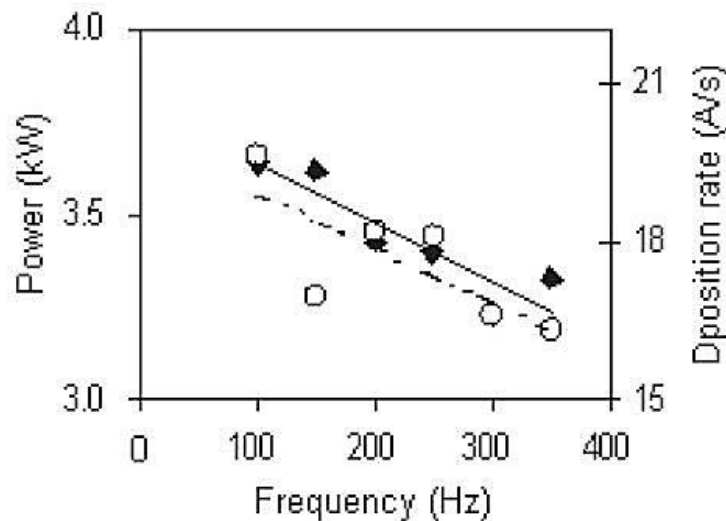


Figure 2.4 Represented by black diamonds is the On-pulsed average power and deposition rate by circles, both as a function of the frequency. Taken from [16]

Chapter 3 **Experimental Procedure**

3.1 **Substrate preparation**

Most of our samples were grown on SiO₂ glass substrates that were prepared for the deposition process in the following manner. First off the substrates needed to be cut from the original 1"x3" (25.4 mm X 7.62 mm) size into smaller squares measuring 0.5" (12.7 mm). This size was mostly dictated by the size of the Peltier heater in the resistance and IR transmittance test chamber, although bigger samples measuring 0.625" (15.7 mm) were made for x-ray diffraction studies. The substrates were then thoroughly cleaned with a solution of detergent (Alconol) and water and, to ensure that there was no detergent residue left on the surface, the substrates were repeatedly rinsed and dried using laboratory wipes. Next, they were placed on 15 ml of Trichloroethylene (TCE) and sonicated for 10 min, followed by 10 minutes in 15 mL of acetone and finally 10 min in 15 mL of methanol. After the methanol sonication the substrates were left to air dry. Followed by the cleaning process the substrates were immediately stored in individual containers to prevent any contamination or scratches to the surface.

After cleaning, the substrates were now ready to be placed inside the vacuum chamber. The substrate was then glued onto a ~5/8" (15.88 mm) and ~1/16" (1.59 mm) thick cooper plate

using flash dry silver paint. The plate and substrate were then glued onto the ceramic heater, again using silver paint, inside the vacuum chamber. Gluing the substrate to a cooper plate instead of directly onto the ceramic heater allows for a more uniform heat distribution on the substrates' surface, which is important because SiO_2 glass is a poor thermal conductor. The paint was allowed to air dry for 10min before rough vacuuming the deposition chamber.

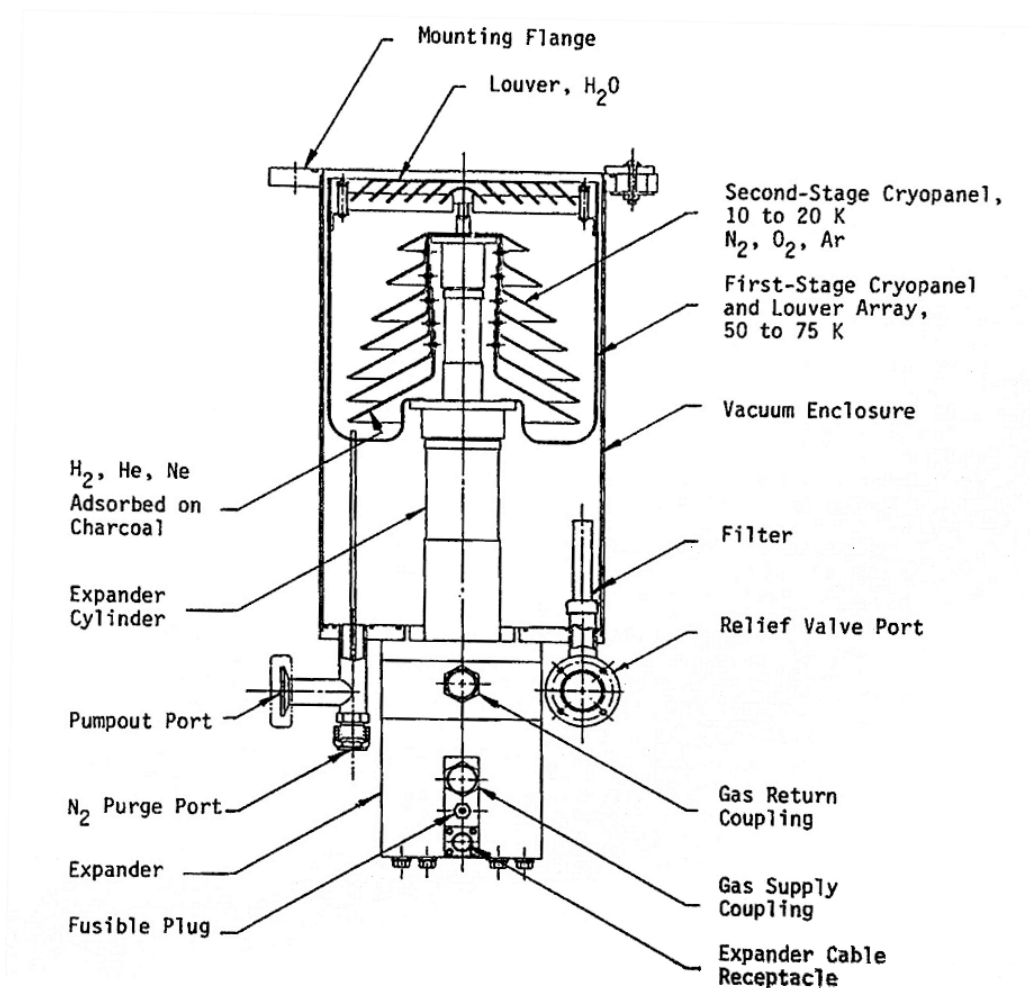


Figure 3.1 Parts identification and stages of cooling during cryopumping [17]

3.2 Helium Cycle Cryogenic Vacuum Pump

Our deposition system uses an APD Cryogenics helium cycle (He-cycle) cryopump as the main vacuum pump and a Varian SD-201 mechanical pump for roughing. Cryopumps are classified as a trapping vacuum pump, meaning that this type of pump traps the air within the body of the vacuum pump itself in contrast to mechanical or many other types of pump which pumps air out of the chamber into the atmosphere. This pump utilizes a two level He compressor and expander to act as a freezer which cools an arrangement of cryopanel onto which the gases will be frozen and trapped. Figure 3.1 shows a cross-section of the type of cryopump used.

The first stage of the expanders cools the outer most cryopanel ultimately reaching a temperature of 50 to 70 K (-223 °C to -203 °C) [17], effectively freezing most of the water vapor present in the deposition chamber (some water vapor will usually remain adhered to surface pores for long times). This first stage of cryopanel also acts as a heat shield between the body of the pump and the second stage of cryopanel.

The second stage of the expander cools down the second stage of cryopanel which reaches working temperature between 20 to 30 K (-253 °C to -243 °C) [17]. This second stage freezes other remaining gases in the chamber mostly oxygen and nitrogen. Remaining gases that are not trapped in the cryopanel are absorbed in a charcoal trap on the cryopanel, although trapping of helium gas, because it is inert and has a very low condensation temperature, is not very efficient. However, since the concentration of helium in the atmosphere is extremely small this is not

problematic. This type of trapping pump is ideal for thin film deposition given the fact that it produces very little or no contamination at all due to hydrocarbons (oil vapors from mechanical pump lubrication) back stream. The fact that a He-cycle cryopump works by trapping air requires the pump to be periodically evacuated of any trapped gases.

3.2.1 Cryopump Regeneration

This procedure was done regularly before the deposition process. The outside of the pump is wrapped in a heating strip connected to a 120 V variable output autotransformer (Variac) which allowed control over the temperature of the heating strip. The outlet of the pump was connected to the mechanical pump through a stainless vacuum steel line, which through a series of valves allowed us to either rough vacuum the deposition chamber or the cryopump. The body of the pump was heated to extract any water condensation accumulated on the cryopanel, while simultaneously been pumped down to a pressure of 30 mTorr. After reaching the desired 30 mTorr pressure, the valve on the pumpout port (see Figure 3.1) was closed separating the mechanical pump from the cryopump. The He compressor was then powered on to cool the cryopump to its working temperature.

3.3 Deposition Chamber Vacuum

Once the cryopump had reached working temperature, the deposition chamber was rough pumped down to a pressure of 20 mTorr using the mechanical pump. After reaching 20 mTorr,

the valve separating the mechanical pump from the deposition chamber was closed and it was then ready to be evacuated to the deposition base pressure using the cryopump. The chamber and the cryopump are separated by a pneumatic sliding gate valve and an iris diaphragm gate valve. The pneumatic gate valve is actuated via a control switch and operated at 60 psi. Once the slide gate is open the pressure inside the chamber drops almost immediately from the original 20 to 100 μ Torr.

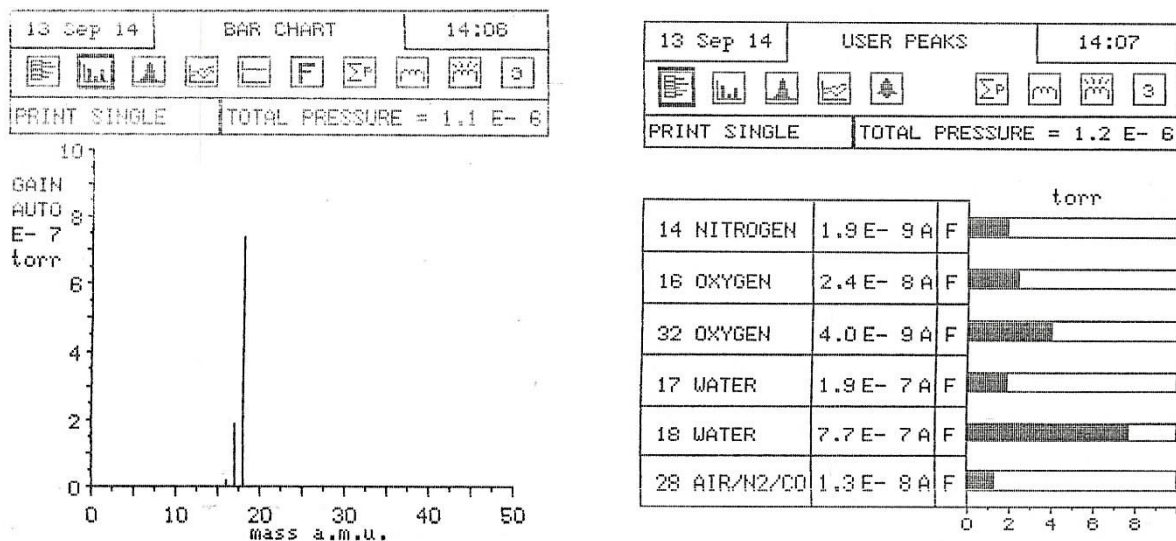


Figure 3.2 Residual gas analysis performed with a Spectra Instrument's Vacscan on the deposition chamber before deposition. Total pressure of the chamber was measured to be 1.1 μ Torr.

At this point the pressure inside the chamber was monitored using a Spectra Vacscan Residual Gas Analyzer (RGA). The system is evacuated until a base pressure of ~ 1.0 μ Torr was reached. Figure 3.2 above shows an example of a residual gas analysis done before each deposition,

where water vapor, followed by nitrogen and oxygen from residual air makes up most of the components of the base pressure.

3.4 Temperature Control

3.4.1 Temperature controller adjustment

The temperature of the ceramic heater inside the deposition chamber, where the substrate was glued, was controlled via a Honeywell UDC 2500 temperature controller. This controller used a K-type thermocouple placed underneath the ceramic heater to measure the temperature of the heater. Since the temperature reading is based on the temperature of the heater instead of the substrate itself, a calibration curve had to be obtained first in order to determine the actual temperature of the substrate during deposition.

Another type-K thermocouple was fitted inside the chamber and connected to an Omega HH-20A High Accuracy Digital Thermometer. The tip of the thermocouple was glued with silver paint to the surface of a substrate which was then glued onto the ceramic heater. The deposition chamber was rough pumped down as if a deposition was to be made. The temperature on the Honeywell controller was increased in 50 °C steps and the autotune function of the controller was enabled. Once a temperature was selected, 5 min were allowed for the temperature to stabilize before recording the substrate's temperature and the controller's temperature readout.

The result of the calibration is shown in Figure 3.3 below. Henceforth, the calibration curve was used to estimate the actual substrate temperature for film growth.

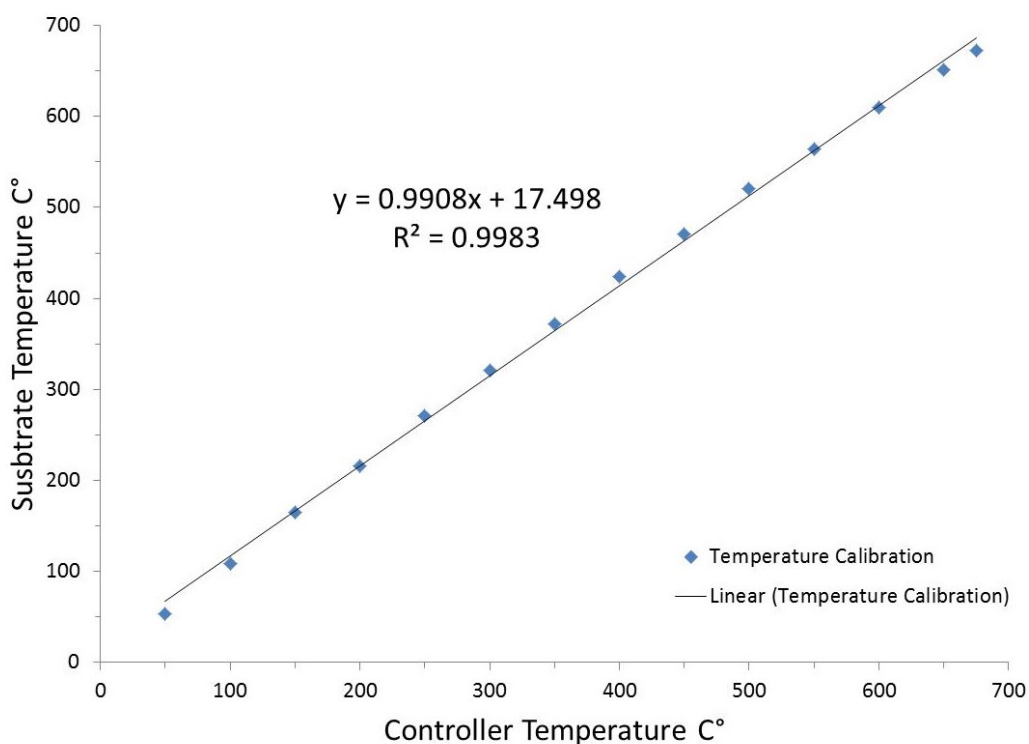


Figure 3.3 Honeywell UDC 2500 temperature controller adjustment graph. The substrate's temperature was obtained with an Omega HH-20A. Both instruments used a type-K thermocouple.

3.4.2 Substrate Heating

Before the deposition process the substrate was heated for 10 min, allowing for a more uniform temperature distribution along the surface of the substrate. Also, since we used the auto tune feature of the Honeywell temperature controller, this permitted the controller to calculate

and adjust control parameters to the chosen temperature without under/over shooting the setpoint or excessive temperature oscillations during deposition.

3.5 Deposition Ar/O₂ Pressure

Deposition was done at a 5.0 mTorr argon atmosphere, but the total pressure of the chamber was varied for different samples. The plasma magnetron sputtering cathode operates, according to the manufacturer, within a pressure range of 0.5 to 100 mTorr [18]. In practice, however, it was not possible to obtain stable operation for more than a few minutes at pressures much lower than 5 mTorr. Therefore, it was decided to use this as the base sputtering pressure. Working with an argon pressure near the minimum practical range of the sputtering cathode assured a greater deposition rate due to lower collision rate between sputtered species and the gas atoms during the sputtering process. After the rough and cryopump vacuum procedures, the argon pressure of the chamber was graduated using the diaphragm valve gate situated between the cryopump and the pneumatic gate valve. At this point, the pressure inside the vacuum chamber was monitored using an Inficon VG-C401 Vacuum Pressure Gauge. The argon flow was kept at a constant 60 ml/min flow using an Aalborg GFM171 Mass Flow Controller. The argon pressure and flow were allowed to stabilize over a period of 5min before oxygen (O₂) was introduced into the chamber.

The oxygen flow was always much lower than the argon flow, so the total pressure is not much higher than the initial 5.0 mTorr value reached with the argon flow. However, the actual oxygen fraction in the chamber atmosphere is known to have a significant effect on the resulting composition of the metal oxides to be deposited. The O₂ flow was adjusted using a Varian 951-5106 leak valve in order to obtain the final deposition pressure on the chamber, and just as it had been done with the argon pressure, the O₂ pressure was left to stabilize for 10 min before deposition.

3.6 Sputtering Process

3.6.1 Plasma Magnetron Cathode

The Onyx-2™ plasma magnetron sputtering cathode used was situated directly above the ceramic heater and substrate, at a distance of 10 cm. This sputtering cathode has a working power limit of 600 W for an RF signal [18], well above the constant 300 W pulsed DC used. The cathode was constantly cooled during and immediately after the deposition by a flow of approximately 1 gal/min of room temperature water at 60 psi. Cooling the sputtering cathode is crucial to prevent the permanent magnets inside the cathode from overheating past their Debye temperature and consequently losing their magnetic properties. These magnets provide a strong magnetic field, confining electrons from the plasma, which enhances ionization and increases bombardment across the target surface. At the same time the water cools the target, but unlike

the magnets, were the water contacts them directly, the water cools a cooper jacket which in turns cools the target. This is known as indirect cooling.

The target itself is a 2" (50.8 mm) round by 1/8" (3.18 mm) thick disk, made of 99.95% pure vanadium disk. A minimum target thickness of 1/4" (6.35 mm) must be used with the Onyx-2™, so a 1/8" (3.18 mm) cooper disk was placed behind the vanadium target as to ensure direct contact with the cooper cooling jacket in order to prevent damage due to overheating of the vanadium target during deposition.

3.6.2 Pulsed DC Signal

The 300 W pulsed DC signal was supplied by an AE Pinnacle® Plus+ Pulsed-DC power supply at a frequency of 150 KHz and an inverse voltage time of 1.5 μ s. These conditions stayed constant through the range of samples produced since they proved to be adequate at preventing excessive charge accumulation on the vanadium target. Charge accumulation on the surface of the target would cause large arc discharges between the cathode body and the target during deposition. This power supply had the capability of producing a square wave of up to 5 kW of power with a reverse time as short as 0.4 μ s. During the reverse voltage time, the Pinnacle® Plus+ supplied a voltage of 10% the value of the voltage used during deposition. For our purposes the Power supplied by the Pinnacle® Plus+ was regulated to the 300 W previously mentioned, consequently the voltage and current values varied per sample as the Pinnacle® Plus+ adjusted to maintain constant power. With the shutter between the cathode and the

substrate closed, the power was initially set to a low 50 W before the output of the Pinnacle® Plus+ was powered on to prevent any sudden power surge as the argon plasma ignited. Once the argon plasma discharge was established, the power was set to 300 W with the shutter still closed.

3.6.3 Vanadium deposition

Due to the polar nature of vanadium, the sputtering target used for deposition is prone to oxidation. Even when exposed to the atmosphere for brief periods of time it is keen to develop a thin oxide layer over its surface. To deal with this oxide layer, the shutter was kept closed for 5 minutes with the argon plasma active (see Figure 3.4 below). This assured that any oxide layer that may have formed over the surface of the vanadium target would be sputtered away rather than be deposited on the substrate. While the material to be deposited is also a vanadium oxide, the change in target surface composition during the initial sputtering phase could have introduced undesirable changes in the composition of the deposited film. After sputter-cleaning the target, the shutter was opened and material was deposited onto the substrate. For the vast majority of the samples deposition was done for a total of 30 min. Figure 3.4 shows the evolution of the film growing atop of a glass substrate; notice the color change of the film as it gradually grows in thickness.

The whitish color of the plasma seen on the images denotes the presence of O₂ injected into the chamber during deposition in order to obtain VO₂. Once the time for the deposition was over, the power output was shut down, the shutter closed and the cooling water ran for an

additional 15 min to cool the target and the magnetron cathode. With the cryopump still running, the oxygen inlet to the chamber was closed but the argon flow was kept for 5 min after deposition to purge the chamber of the remaining O_2 and prevent further oxidation of the sample while it cooled off.

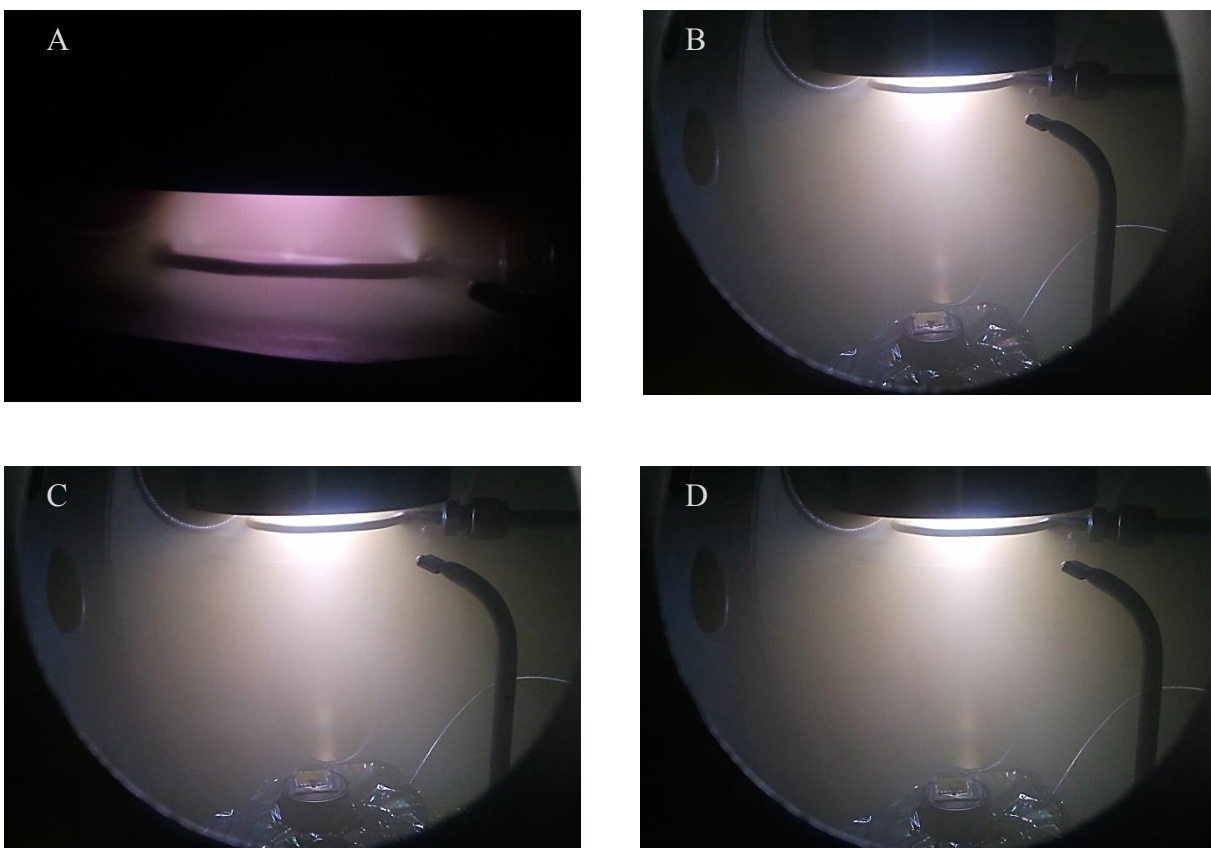


Figure 3.4 A) Sputtering while the shutter was closed in order to clean substrate's surface. B) Vanadium deposition on glass substrate after 5 minutes of deposition, B) 10 minutes and C) 15 minutes.

3.7 Sample Annealing

Some samples were selected for an annealing process in order to observe variation on the crystal structure of the deposited films. The process was done *in situ* after deposition following annealing conditions derived from literature revision [19]. After deposition, the temperature of the sample was raised to 450 °C while oxygen was reintroduced into the chamber in order to promote further oxidation of VO_x into VO₂. The flow of oxygen (O₂) within the chamber was controlled with the mechanical pump and the Varian leak valve to ensure that the flow of oxygen coming into the chamber and the gas flow being pumped out would maintain a constant pressure of 250 mTorr. Just like it was done after the deposition, once the annealing process was over, the chamber was flushed with argon until the sample cooled to at least 150 °C. The first annealed samples were submitted to this treatment in time intervals of 15, 30 and 45 min. The 30 min sample showed the best results for the annealing process, meaning that it showed a better transition in electrical resistance and infrared transmittance. After 30 min of annealing the samples did not show improvement in their electrical and optical properties. Therefore the rest of the samples were annealed for a maximum time of 30 min.

3.8 Sample Thickness

After deposition and annealing the samples were removed from the deposition chamber and carefully cleaned to remove any silver paint residue adhered to the back of the substrate. Before

the deposition, a small piece of silicon wafer had been glued to the rim of every sample (see Figure 3.4 B). After the deposition and annealing, the small silicon piece was removed, leaving a small step on the edge of the sample. This step was then used to measure the thickness of the vanadium film deposited using a Tencor Alpha-Step 100 profilometer. This instrument is a contact profilometer which works by sweeping the surface of the sample with a small stylus which is accurately balanced on a long boom. As the stylus moves across the surface, any movement due to the surface profile is reflected at the far end of the boom. The movement is then amplified by the electronics and recorded onto a scaled graph paper as shown in Figure 3.5 below.

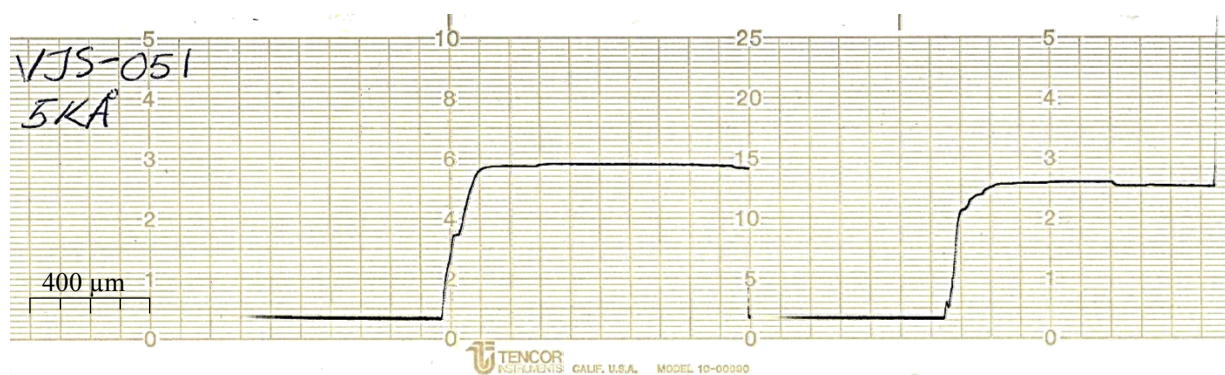


Figure 3.5 Profilometer graph for a vanadium deposition, as recorded by a Tencor Alpha-Step 100, using a 5000 Angstrom ($5 \text{ k}\text{\AA}$) scale setting.

The thickness of the film is then determined by calculating the ratio between the measured step and the full graph scale. Going back to Figure 3.5, the step is measured at 26 mm, therefore:

$$\left(\frac{26 \text{ mm}}{50 \text{ mm}}\right) \times 5000 \text{ \AA} = 2600 \text{ \AA} \quad (3.1)$$

The steps were made wide enough in order to be able to measure multiple times on different locations. Final thickness of the film was determined by averaging the measurements.

3.9 Vanadium Oxide Transition Testing

When VO_2 is heated above $68 \text{ }^\circ\text{C}$ it undergoes a semiconductor-to-metal transition (SMT). This transition is accompanied by changes in the transmittance of infrared (IR) light and the electrical resistance of the thin film. Figure 3.6 below shows a diagram of the experimental arrangement of the equipment setup used to test the dependence on temperature of these properties.

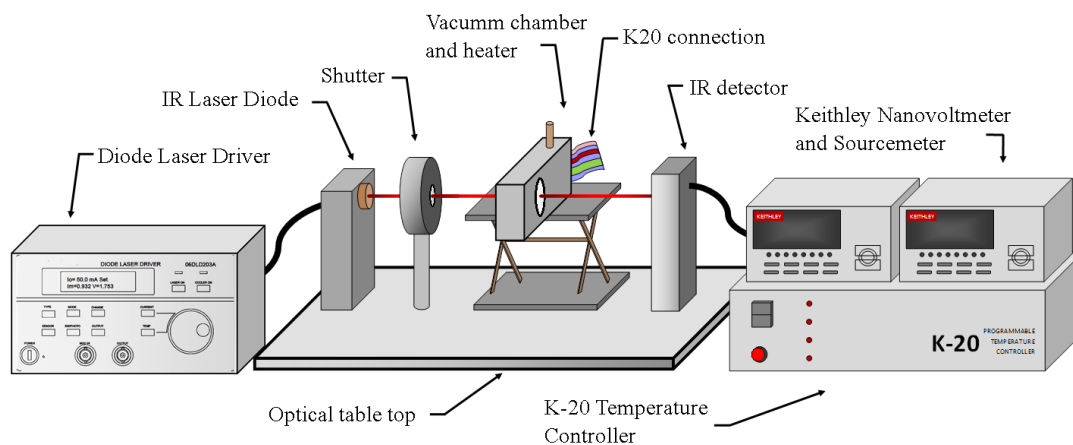


Figure 3.6 Experimental setup for optical IR transmittance and electrical resistance testing of vanadium samples.

3.9.1 Optical Transition

As the deposited sample is heated, the transmittance percentage slowly decreases, but when reaching the transition temperature the transmittance drops abruptly. To test this phenomenon, the sample was glued onto a ceramic heater controlled with a MMR Technologies K-20 temperature controller. The heater has a small perforation to allow a laser beam to pass through the sample. The heater itself is placed within a small vacuum chamber with Pyrex windows through which a Mitsubishi ML series IR laser is shined. The laser operates at a constant power output controlled by a DLD 203 Melles Griot Precision Diode Laser Driver. On the other side of the chamber lies a Thor Labs IR intensity detector. The IR detector outputs a DC voltage signal which is read by a Keithley 2182 Nanovoltmeter.

In order to keep the vanadium sample from heating from exposure for extended periods of time to the IR laser used to measure transmittance, a Uniblitz® electronic shutter was placed between the IR laser and the sample holder. With this setup, once the temperature stabilizes the shutter opens for a brief period of time, the computer takes various measurements and the shutter closes again until the temperature controller takes the sample to the next temperature setpoint and stabilizes it.

3.9.2 Electrical Resistance

The electrical resistance of the sample was measured simultaneously while the IR transmittance test was run. For the electrical connections, two #36 AWG gold wires were attached to the surface of the sample using pressed indium (In) metal contacts. The wires were then connected to a Keithley 2400 sourcemeter through a pair of feedthroughs on the vacuum chamber. The whole connection was measured at 3.4 Ω of resistance, which was negligible, as the majority of the samples themselves showed resistance values upwards of 500 Ω after transition and higher than this at lower temperatures.

3.9.3 LabVIEW Software

The experimental setup (Figure 3.6) was remotely controlled from a Windows XP PC running LabVIEW. The software was purposely developed as part of this work to provide reliable and consistent means of measuring the dependence of the vanadium oxide samples electrical and optical properties on temperature. The software allows the user to enter a Setpoint temperature and a Temperature Step, these temperature parameters are sent to the K-20 temperature controller which will ramp the temperature of the sample while providing a constant, on-screen, temperature readout (see Figure 3.7). Additional time parameters marked as Heating Delay Time and Cooling Delay time allows the user to enter waiting times for the up and down heating ramps times independently.

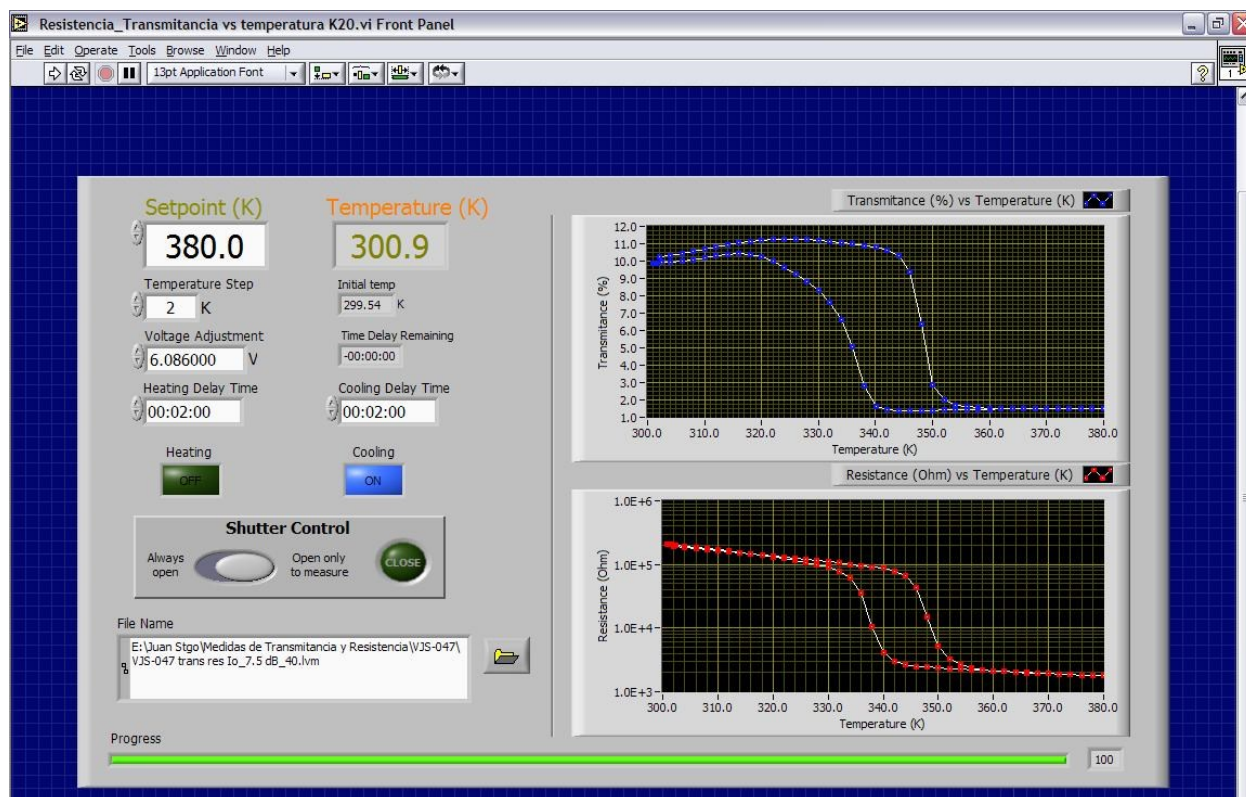


Figure 3.7 LabVIEW software user interface (Front Panel).

These time delays ensure that the temperature of the sample stabilizes before measurements are taken. Temperature stabilization was found to be related to the substrate size and thickness. A calibration curve was done to ensure correct temperature readout. A calibration curve (Figure 3.8 below) was done by silver gluing a substrate on the heater and on top of the substrate a K-Type thermocouple which was then connected to a handheld Omega thermocouple readout.

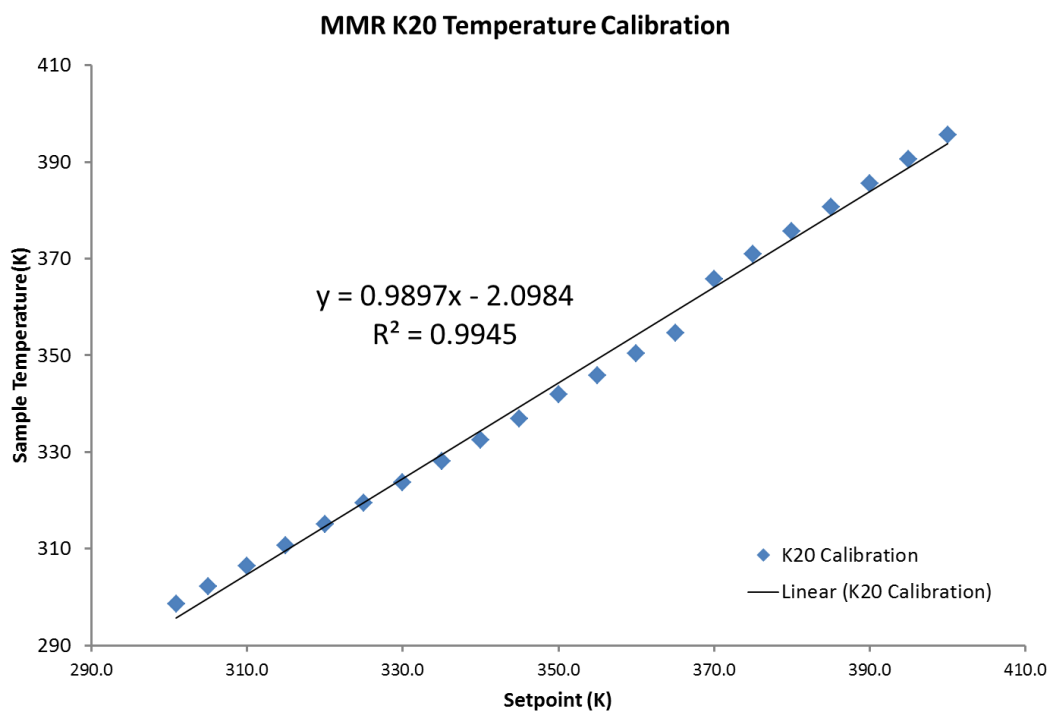


Figure 3.8 Temperature Calibration on MMR K20 temperature controller.

In addition to the resistance measurements, the software and experimental setup allowed for simultaneous measurements of IR transmittance of the vanadium oxide samples. Since the samples were placed inside the small vacuum chamber (Figure 3.6), the IR laser beam passed through two Pyrex windows before arriving at the IR sensor. Therefore a calibration was needed in order to take into account the base reflectivity of the system, including reflectivity due to the substrate itself. The Melles-Griot laser controller allowed for laser intensity adjustment on a

scale from 5.0 to a maximum of 14.0 W. In addition the IR sensor allowed the signal output to be amplified on a range from 0 to 70 dB. Since the transmittance of the sample varied according to the sample's thickness, different laser output and signal amplification settings were used per sample. Therefore, the transmittance calibration was performed for all possible combinations between the laser controller's power output and the IR amplifier range. The result of this calibration (see Appendix A.1) could then be entered by the user into the software using the Voltage Adjustment tab.

Once all parameters had been entered, the program could be started. The program's graphical user interface (GUI) provided the user with feedback while the measurements were made. A live temperature read out was displayed and labeled as Temperature (K). On the right hand side the Transmittance (%) vs Temperature and Resistance (Ohm) vs Temperature (K) graphs were built and displayed as the data was acquired. Additional user feedback was provided by a Progress bar at the bottom of the front panel.

As data points were acquired the program, apart from displaying the measurements live, would create a text document and store it in a file location selected on the front panel by the user. The file is a text file with LabVIEW *.lvm (LabVIEW measurement) extension. Data within the file is tab delimited, meaning the resistance, transmittance and temperature data points were arranged in three columns separated by tabs. The file could then be accessed with any text editor or spreadsheet application. Table 5.2 on Appendix A.2 shows an example of a file produced by the program.

Chapter 4 Results and Discussion

All of the electrical and optical characterization results discussed in this chapter were obtained via the methods presented in the previous chapter. Additional results are presented for X-ray diffraction (XRD) and atomic force microscopy (AFM). A total of 56 samples were fabricated during the development of this work, with the most salient results discussed here. Parameters such as overall deposition pressure (p_d), argon partial pressure (p_{Ar}), oxygen partial pressure (p_{O_2}) and deposition temperature (T_d) were varied in order to optimize results (Table 4.1 below).

Parameter	Range
Partial Oxygen Pressure	0.2 – 0.8 mTorr
Total deposition pressure	5.2 – 6.0 mTorr
Deposition Temperature	325°- 650°C
Annealing time	15 – 45 min

Table 4.1 Deposition parameter range.

The Pulsed-DC parameters were continued as in previous work [15], as these conditions proved to be successful in preventing excessive arcing on the surface of the target, associated

with charging of the dielectric surface which develops on the target surface as sputtering proceeds. Other parameters were varied in order to seek improved quality of the films.

Some of these deposition parameters were limited in part due to technical specifications discussed in the previous section. For the first group of samples parameters were kept as close as possible to the conditions used by Torné. For the first set of samples the deposition temperature was kept constant at 650°C, and argon and oxygen partial pressures were kept at 5.0 mTorr and 0.3 mTorr respectively. The vacuum chamber was fitted with an argon gas inlet line which let argon directly into the face of the sputtering gun and target surface. A second gas inlet was fitted to inject oxygen halfway between the sputtering gun and the substrate holder. Various samples were fabricated, with varying combinations between the gas inlets. Although none of the first samples produced VO₂, as determined by electrical resistance testing, it was noted that the deposited material was much more abundant when both inlets were installed. The thickness of the samples could not be determined since the surface of the substrate used warped during deposition.

After evaluating the first set of results it was decided to deposit at much lower temperature to avoid warping the glass substrates. It was also evident, by the low resistance of the samples produced, that the oxygen pressure needed to be increased. Following these initial adjustments, better results were obtained, which are presented in section 4.2.

4.1 Deposition Parameters

To determine these parameters, depositions were carried out gradually reducing the deposition temperature (T_d) until the glass substrate was uniformly covered by deposited material. Judging by the color of the deposited film and the small changes in electrical and optical properties obtained during characterization, the material deposited appeared to have been mostly a mix of different vanadium oxides phases with very low traces of VO_2 . Therefore the next step was to gradually step up p_{O_2} . Table 4.2 presents a summary of the parameters with the most significant results. These set of samples allowed for analysis on the effects of deposition temperature and annealing time on the electrical and optical properties of the thin films.

Sample	Base Pressure (μTorr)	p_{O_2} (mTorr)	T_d ($^{\circ}\text{C}$)	Thickness (Angstrom)	Annealing		
					Time min	T ($^{\circ}\text{C}$)	p_{O_2} (mTorr)
VJS-024	1.00	0.45	414	4,000	No annealing		
VJS-036	1.20	0.50	354	2,225	No annealing		
VJS-038	1.20	0.50	360	1,900	20	463	250
VJS-047	0.61	0.50	360	2,300	30	463	250
VJS-040	1.20	0.50	360	2,400	45	463	250
VJS-041	1.20	0.50	360	1,375	30	463	250
VJS-042	1.20	0.50	360	1,000	30	463	250

Table 4.2 Deposition parameters for most relevant results. For all samples, the argon deposition pressure was kept at 5.0 mTorr.

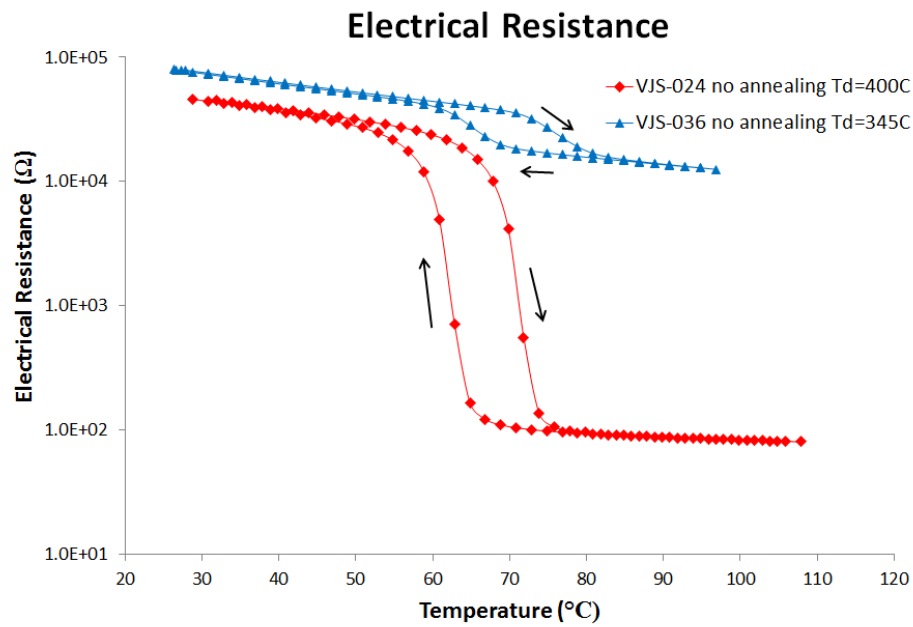
4.2 Electrical Resistance and IR Transmittance Results

4.2.1 Effects of Deposition Temperature

All electrical testing and IR transmittance measurements were done using the LabVIEW program developed during this work. Samples VJS-024 and VJS-036 showed the best contrasting results for comparing the effects of deposition temperature (T_d) on the electrical and optical properties on the non-annealed thin films. Overall, sample VJS-024 showed the best result for changes during IMT phase change. This sample exhibited a change of three orders of magnitude in electrical resistance. However we were unable to repeatedly obtain as good of a result using the same deposition parameters. After incorporation of the annealing process, results, although not as good as for VJS-024, were certainly more consistently repeatable.

VJS-024 and 036 were deposited with near identical conditions, but varying the deposition temperature by 40°C. The results of this variation on the samples characteristics are shown in Figure 4.1. Despite the fact that both samples start with similar resistance values at room temperature, the hotter deposition exhibits a much higher transitional jump in electrical resistance and IR transmittance as well.

A)



B)

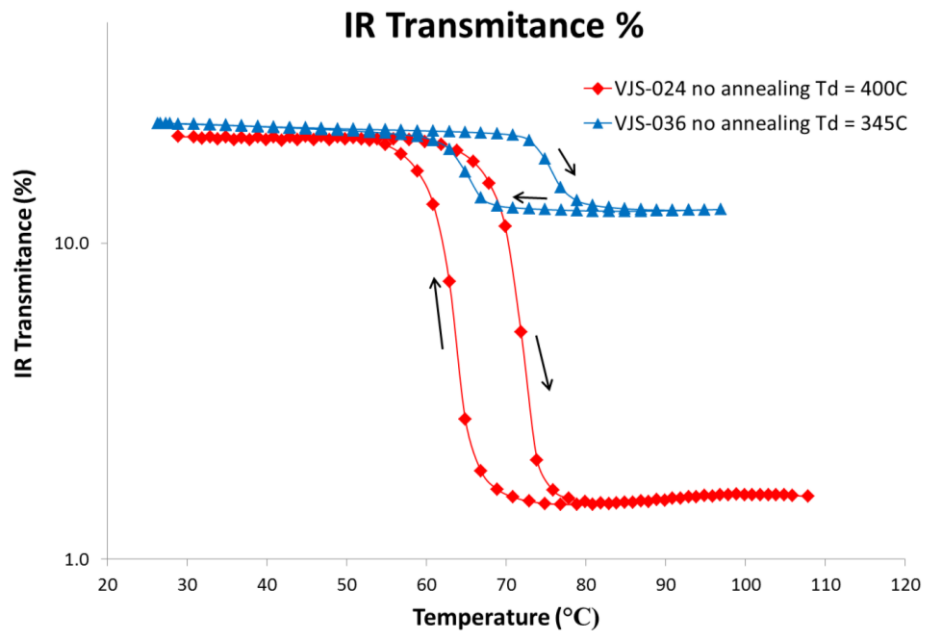


Figure 4.1 A) Electrical resistance and B) Infrared transmittance of samples without annealing process. Arrows show direction of the heating cycle.

To determine the temperature at which the ITM transition occurred (T_t), the data obtained was processed on a spreadsheet application to calculate the slope between each two consecutive data points. The T_t is then determined by the midway temperature between the points with the highest slope. Details about the changes in resistance and transition temperature of these two samples are summarized in Table 4.3. Sample VJS-024 goes through the phase transition 5 °C earlier in the heating ramp and 3°C earlier on the cooling ramp. Both samples showed similar hysteresis width, with VJS-036 being just 1 °C wider in both tests.

Sample	R_{max} (Ω)	R_{min} (Ω)	Max t_{IR} (%)	Min t_{IR} (%)	Heating T_t ($^{\circ}\text{C}$)	Cooling T_t ($^{\circ}\text{C}$)
VJS-024	4.59E+04	8.03E+01	21.79	1.49	67	56
VJS-036	7.95E+04	1.25E+04	24.01	12.64	73	61

Table 4.3 Electrical and optical characterization results for non-annealed samples.

4.2.2 Effects of Annealing

To study the effects of the annealing process on the deposited films, samples VJS-038, 047 and 040 were annealed for periods of 20, 30 and 45 min respectively. The annealing temperature and O_2 pressure were kept at a constant 450°C and 250 mTorr, this conditions are based on those

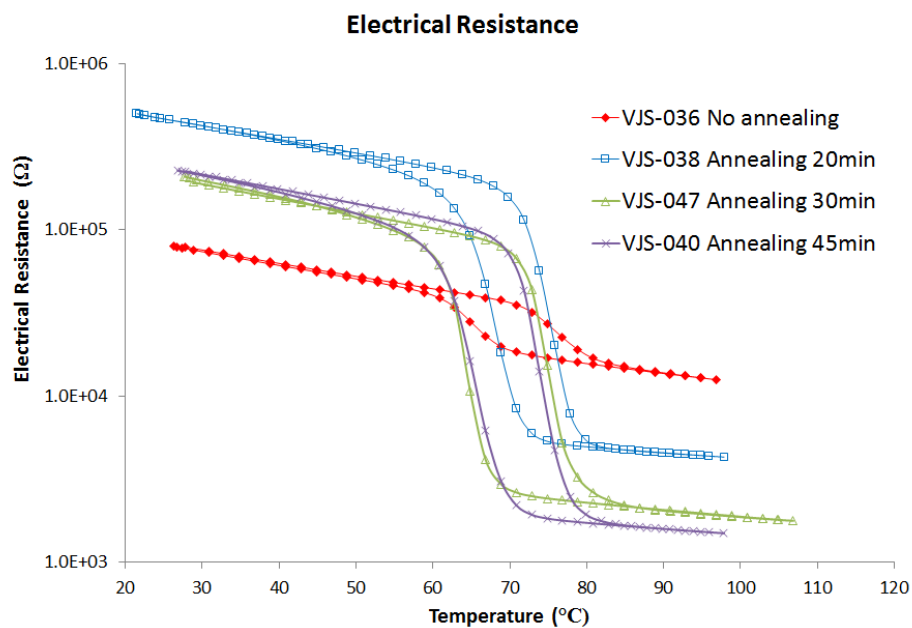
presented by J.Y. Suh *et al.* in their work on VO₂ deposition [19]. Figure 4.1 portrays the effects of different annealing times on samples grown under the same deposition parameters (Table 4.2).

Table 4.4 below details the results from the graphs shown in Figure 4.2, with the exception of VJS-036 which is already presented on Table 4.3. Comparing the results of the annealed samples with the non-annealed sample VJS-036, a noticeable improvement is seen in the magnitude of the change in electrical and optical properties of each sample. The resistance ratios R_{\max}/R_{\min} as well as the transmittance ratios $t_{\text{IR}}^{\max}/t_{\text{IR}}^{\min}$ for the annealed samples also shows steady improvement as the annealing time was increased.

Sample	R_{\max} (Ω)	R_{\min} (Ω)	R_{\max}/R_{\min}	t_{IR}^{\max} (%)	t_{IR}^{\min} (%)	$t_{\text{IR}}^{\max}/t_{\text{IR}}^{\min}$	Heating T_i ($^{\circ}\text{C}$)	Cooling T_i ($^{\circ}\text{C}$)
VJS-038	4.99E+05	4.29E+03	116	14.80	2.56	5.78	71	62
VJS-047	2.09E+05	1.77E+03	118	11.26	1.39	8.10	72	58
VJS-040	2.27E+05	1.49E+03	152	18.24	2.18	8.36	71	58

Table 4.4 Electrical and optical characterization results for annealed samples. Shaded columns depict the change on the magnitude of the phase transitions.

A)



B)

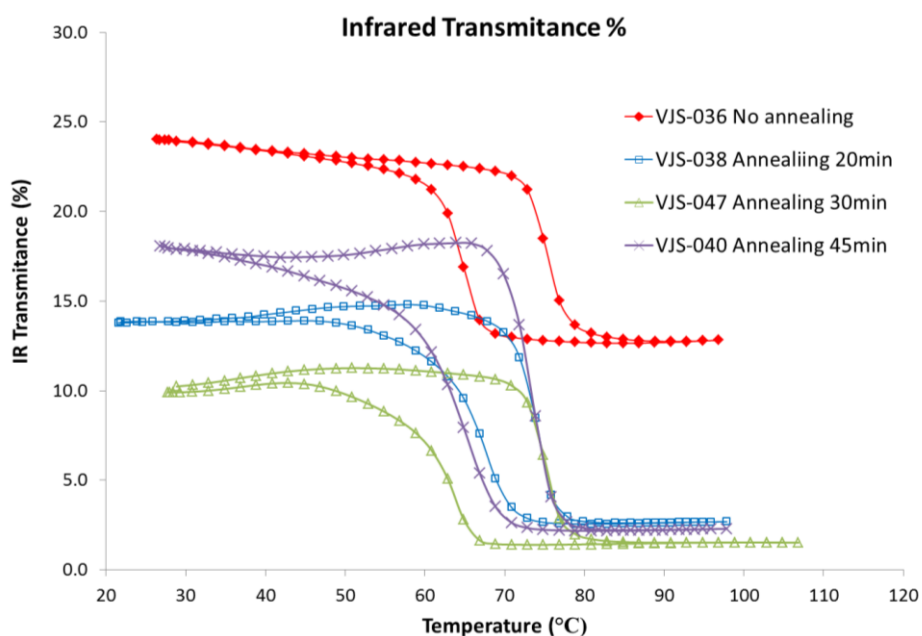


Figure 4.2A) Electrical resistance and B) Infrared transmittance of samples grown under same conditions but subjected to different annealing times. Heating cycle follows same paths as in Figure 4.1.

All of the annealed samples showed comparable values of T_i between them, which can also be said when comparing to the non-annealed sample VJS-036 whose T_i was measured at 75 °C with a hysteresis width of 12 °C. When comparing results for the as-deposited and annealed samples, it is established that both samples VJS-024 and VJS-040 produce similar results in electrical and optical transitions. Their hysteresis widths differ by only 1 °C. The annealing process, however, seems to have shifted the T_i by as much as +5 °C for the heating ramp and +6 °C for the cooling ramp.

4.3 XRD Results

XRD analysis was carried out on sample VJS-036 and samples with time variation in the annealing process to determine the effects of annealing on the crystal structure. The deposition parameters for all the samples discussed in this section can be found in Table 4.2, Section 4.1, with the exception of sample VJS-039 whose deposition parameters were identical with VJS-047. Figure 4.3 shows the combined results for the XRD analysis. During the electrical and optical testing, VJS-036 showed the presence of small quantities of VO₂. XRD results further confirms this by a small, but noticeable, diffraction peak near $2\theta = 27.8^\circ$, close to the position for the VO₂ reflection corresponding to the (011) plane for the VO₂ monoclinic phase [20].

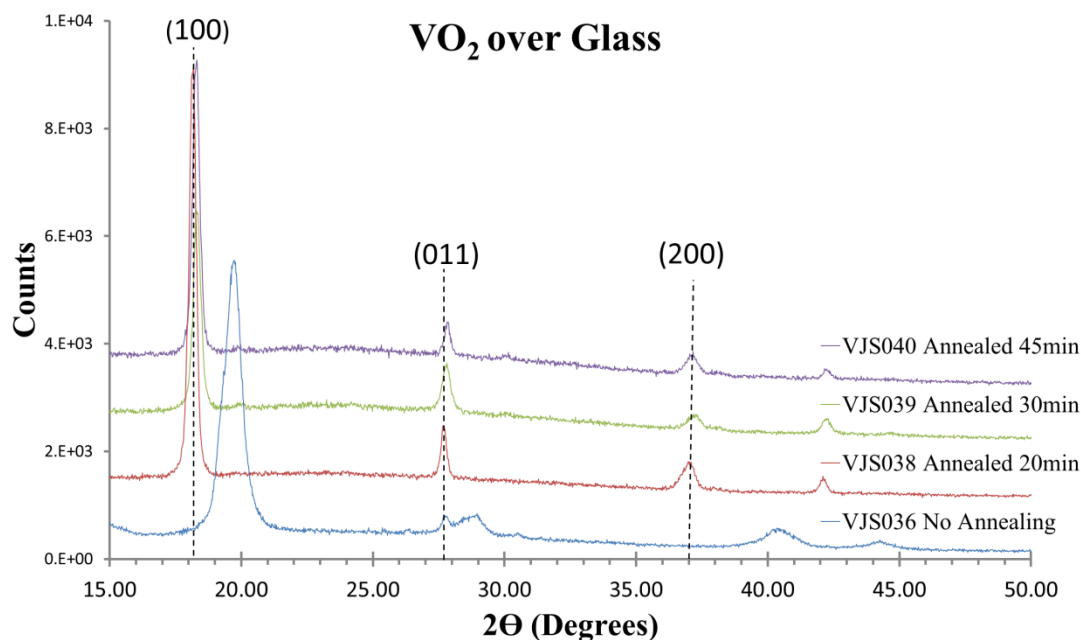


Figure 4.3 XRD results for VO₂ samples.

The annealed samples VJS038 and 040 also exhibit this diffraction peak, even with higher intensity than the non-annealed sample. All the annealed examples, even VJS-038, which was annealed for the shortest period, exhibit a strong preference to align with the (100) plane parallel to the substrate surface, as shown by a very prominent diffraction peak at $2\theta = 18.29^\circ$. The second order peak, corresponding to (200) reflection, can also be seen at $2\theta = 37.0^\circ$. The alignment for the annealed samples is by no means perfect, as diffraction peaks can also be seen at $2\theta = 27.8^\circ$ and $2\theta = 42.3^\circ$, which corresponds to VO₂ with crystals aligned with the (011) plane parallel to the surface. The diffraction peak widths for the annealed samples show small variations between them, indicating that the samples have different crystal sizes.

For the annealed samples, the distance between (100) planes can be calculated from the Bragg equation:

$$2d \sin \theta = \lambda \quad (4.1)$$

$$d = \frac{(1.54)}{(2 \cdot \sin(9.145))} = 4.84 \text{ \AA} \quad (4.2)$$

This value should concur with the separation between (100) planes, which intersect the a axis at an oblique angle in this monoclinic structure. This distance can be calculated from the lattice constants for monoclinic VO₂ given by [20]. In particular, the required lattice constants are $a = 5.75 \text{ \AA}$ and $\beta = 122.6$. Then, from the measured Bragg angle:

$$d = 5.75 \cdot \cos(122.6) = 4.84 \text{ \AA} \quad (4.3)$$

Based on the width of the refraction peaks, the average crystal grain size for each sample in a direction normal to the sample surface can be calculated using Scherrer's equation,

$$\tau = \frac{0.94 \cdot \lambda}{b \cdot \cos(\theta)} \quad (4.4)$$

where b stands for the full width of the refraction peak at half its maximum height (FWHM), θ is the Bragg angle for the peak, λ is the wavelength of the radiation used (1.45 Å in our case), and the numerical constant is a parameter or order 1 which actually depends on the shape of the crystals and is often taken to equal 0.94 for the present purpose.

Annealing time (m)	FWHM (Degrees)	Grain Size (nm)
20	0.295	28.75
30	0.300	28.19
45	0.315	26.65

Table 4.5 Grain size for annealed samples based on the XRD results.

Table 4.5 presents the values for grain size based on this calculation. Results show that the grains changed their size only slightly as the annealing time was increased and, in any case, reduced their size. It is emphasized that the grain size estimated by the Scherrer equation corresponds to the direction perpendicular to the plane (100). It contains no information about the lateral size of the crystal grains.

The presence of VO₂ diffraction peaks for the desired M phase does not necessarily translate into good electrical and optical qualities. These two qualities are highly dependent on the stoichiometry of the material. Figure 4.4 shows a comparison for samples VJS-041 and 042, both deposited under the nominally identical conditions, but VJS-042 was annealed *in situ* after deposition. The XRD results show similar VO₂ diffraction peaks, just as before, but the electrical and optical properties of the samples are significantly altered by annealing. The annealing process allows for any remaining VO_x to evolve into VO₂ and so enhancing the electrical and optical properties.

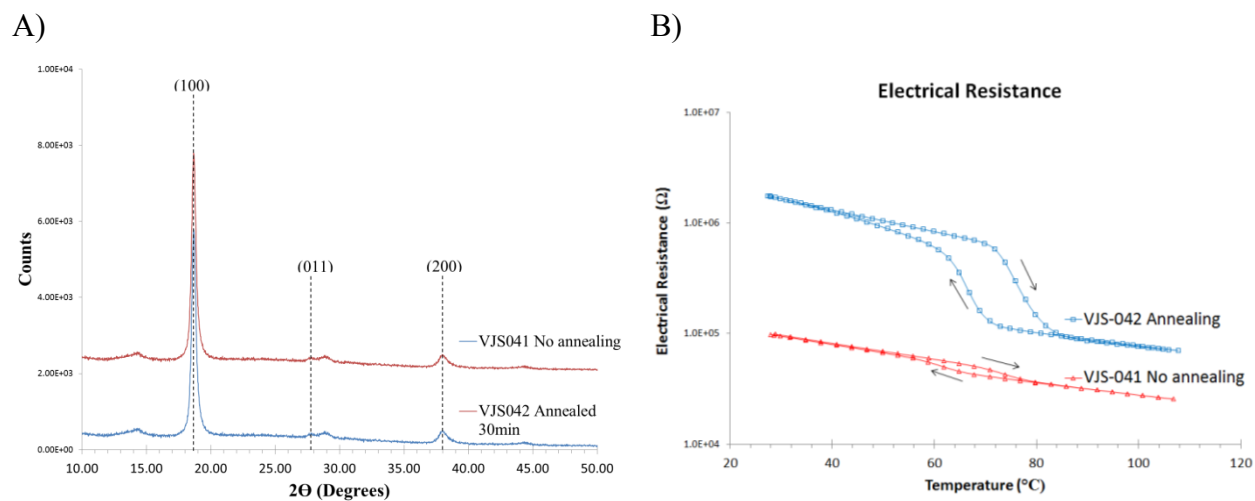


Figure 4.4 A) XRD comparison for not annealed and annealed sample. B) Electrical resistance testing for same samples.

4.4 AFM Imaging

Annealed samples were analyzed by atomic force microscopy (AFM) to study the effects of annealing times on the substrate surface and lateral grain size. Table 4.6 presents the results for the surface roughness analysis, average and average grain size for each sample.

Annealing time (minutes)	RMS Roughness (nm)	Average lateral grain size (nm)
20	16.50	110
45	26.10	300

Table 4.6 AFM Roughness results for annealed samples VJS-38 and 040.

AFM images show a noticeable increase on lateral grain size between samples annealed for 20 min and the sample annealed for 45 min. These results are similar to those published by Suh *et al.* on VO₂ annealing and grain size [19]. Our electrical testing results showed that the sample with the less annealing time, and therefore smaller grain size, had the smallest resistance drop during the SMT of all annealed samples (refer to Table 4.4 on page 44). Films with smaller grains have more grain boundaries which creates imperfections in the VO₂ film and therefore limiting the conductivity during the metal phase due to electron scattering. Contrary to this, as the grain size grows with the annealing process, the grain boundaries decrease, giving way for less resistance on the film on the metallic phase and thus allowing for a more abrupt resistance drop as shown in section 4.2.2.

Upon closer inspection of AFM results for the sample with 45 minutes annealing time (VJS-040) we can find traces of what used to be the smaller grains merging into the bigger grains. This is more evident on the surface profile graph where the bigger peaks (bigger grains) show smaller peaks (small grains) within their contour. This implies that annealing times above 45 minutes could further improve the sample uniformity, thereby positively affecting the electrical transitions.

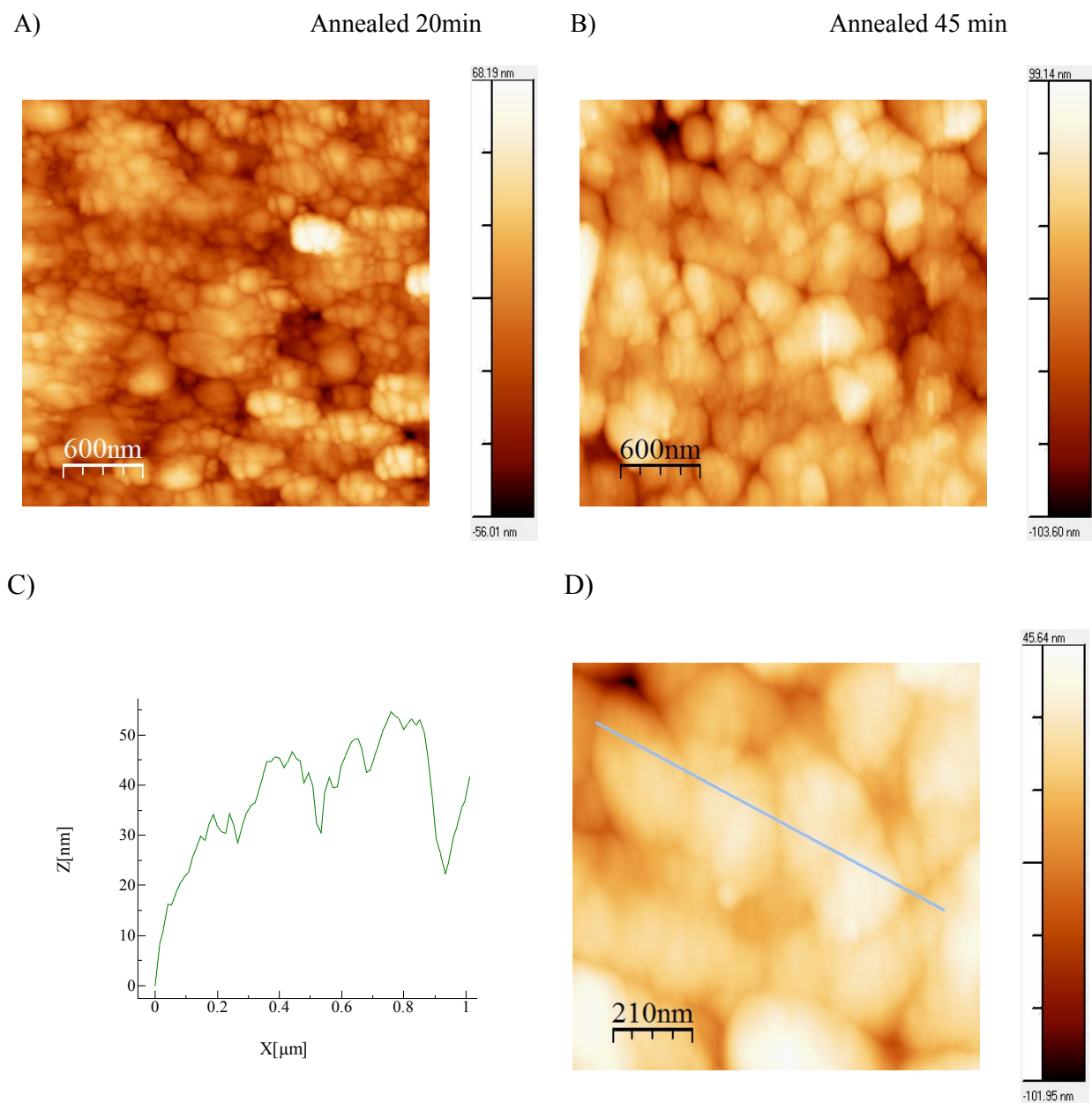


Figure 4.5 AFM images for A) VJS-038 and B) VJS-040. C) Surface profile of VJS-040 along the line shown to the right. D) Close up for AFM results of VJS-040. Images processed using WSxM [21].

Chapter 5 Conclusion

We were able to achieve successful conditions for depositing monoclinic VO₂ thin films on glass substrate by implementing the use of Pulsed-DC reactive sputtering. Using partial pressures as low as 5.0 mTorr and 0.45 mTorr for argon and oxygen respectively and a power of 300W on the sputtering gun, we achieved average deposition rates of 24.5 Å/min. Pulsed-DC parameters of 150 KHz and inverse times of 1.5 μs proved adequate for preventing arcing during deposition due to charge accumulation on the target's surface. With a deposition temperature of 414 °C we were able to observe a sample which showed an impressive 3 magnitude resistance drop and a reduction of 16% on infrared transmittance during characterization. However, conditions for recreating these results proved to be challenging due to the difficulty with partial oxygen pressure control at the low values required, which fluctuated around 0.5± 0.10 mTorr. Electrical and optical properties of the VO₂ are highly dependent on correct stoichiometry, therefore the oxygen control during deposition is highly important.

The annealing process was introduced to the fabrication to further improve the electrical and optical properties of the film by allowing the remaining VO_x on the thin films to evolve into VO₂. After annealing the samples *in situ* after deposition for as low as 20 minutes at a temperature of 463 °C in an oxygen environment at 250 mTorr the samples showed

improvement on the characterization tests. The electrical and optical results repeatability also improved after annealing. As XRD tests showed, samples without annealing showed M-phase VO₂ diffraction peaks but performed poorly on the electrical and optical results. Besides the likely improvement in stoichiometry, annealing also increased the lateral grain size of the films, which can also contribute to improved electrical and optical properties.

For the non-annealed samples, VJS-024 showed the best results during electrical and optical testing. During the phase transition exhibit a resistance ratio $R_{\max}/R_{\min} = 5.67 \times 10^3$ and an optical IR transmittance ratio of $t_{\text{IR}}^{\max}/t_{\text{IR}}^{\min} = 14.62$. Both characteristics underwent a sharp hysteresis loop ~ 11 °C wide located at 67 °C for the heating cycle and at 56°C for the cooling cycle. This sample was deposited at 414°C with an oxygen partial pressure of 0.45 mTorr while the argon pressure was kept at 5.0 mTorr. The results of these sample however prove difficult to recreate due to the high precision require for oxygen control during deposition.

For the annealed samples, VJS-040 exhibited the best phase transition results with a $R_{\max}/R_{\min} = 1.52 \times 10^2$ and $t_{\text{IR}}^{\max}/t_{\text{IR}}^{\min} = 8.36$. The hysteresis, with a width of 13°C, appeared to have shifted to a higher temperature as it was located between 71°C and 58°C for the heating and cooling cycles respectively. This sample was deposited at a lower 360°C while the partial oxygen pressure was 0.50m Torr and argon working pressure 5.0 mTorr. After deposition the samples was annealed *in situ* for 45 min at 463°C in an oxygen pressure of 250 mTorr.

Better samples can be obtained if a more precise and constant oxygen pressure control system can be implemented. Increasing the deposition parameters values could also benefit the oxygen control by allowing the equipment to work on a more stable range. From the AFM results it was noted that the samples could be annealed for longer periods of time, allowing for a more uniform grain size and therefore reducing the grain boundary density.

A software program for this work using the LabVIEW platform and interfacing with all instruments for electrical and optical characterization was developed as user friendly software that will now be available for future work with these and other types of thin films. The software provides faster and more reliable data acquisition.

References

- [1] F. Morin, "Oxides which show a metal to insulator transition at the Neel temperature," *Physical Review Letters*, vol. 3, no. 1, pp. 34-36, 1959.
- [2] J. Nag and R. F. Haglund Jr, "Synthesis of Vanadium Dioxide Thin Films and Nanoparticles.," *Journal of Physics: Condensed Matter*, vol. 20, no. 26, 2008.
- [3] S. Lysenko, V. Vikhnin, F. Fernández, H. Liu and A. Rúa, "Photoinduced insulator-to-metal phase transition in VO₂ crystalline films and model of dielectric susceptibility," *Physical Review B*, vol. 75, no. 7.
- [4] S. Lysenko, A. Rúa, V. Vikhnin, F. Fernández and H. Liu, "Insulator-to-metal phase transition and recovery processes in VO₂ thin films after femtosecond laser excitation," *Physical Review B*, vol. 76, no. 3.
- [5] R. Lopez, T. E. Haynes, L. A. Boatner, L. C. Feldman and R. F. Haglund Jr., "Size effects in the structural phase transition of VO₂ nanoparticles," *Physical Review B*, vol. 65, no. 22, 2002.
- [6] E. N. Fuls, D. H. Hensler and A. R. Ross, "Reactively Sputtered Vanadium Dioxide Thin Films," *Applied Physical Letters*, vol. 10, p. 199, 1967.

- [7] C. Leroux and G. Nihoul, "From VO₂(B) to VO₂(R): Theoretical structures of VO₂ polymorphs," *Physical Review B*, vol. 57, no. 9, 1998.
- [8] F. Théobald, "Étude hydrothermale du système VO₂-VO_{2,5}-H₂O," *Journal of Less Common Metals*, vol. 53, no. 1, pp. 55-71, 1977.
- [9] Y. Oka, T. Yao and N. Yamamoto, "Structural phase transition of VO₂(B) to VO₂(A)," *Journal of Materials Chemistry*, vol. 1, no. 5, 1991.
- [10] F. Morin, "Oxides which show a metal to insulator transition at the Neel," *Physical Review Letters*, vol. 3, no. 34, 1959.
- [11] F. J. Morin, "Oxides of the 3d Transition Metals," *The Bell System Technical Journal*, vol. 37, pp. 1047-1084, 1958.
- [12] A. S. Barker, H. W. Verleur and H. J. Guggenheim, "Infrared Optical Properties of Vanadium Dioxide Above and Below the Transition Temperature," *Physical Review Letters*, vol. 17, 1966.
- [13] H. W. Verleur, A. S. Barker and C. N. Berglund, "Optical Properties of VO₂ between 0.25 and 5 eV," *Physical Review Letters*, vol. 172, p. 788, 1968.
- [14] E. Kusano, J. A. Theil and J. A. Thornton, "Deposition of vanadium oxide films by direct-current magnetron reactive sputtering," *Journal of Vacuum Science & Technology A*, vol. 6, pp. 1663-1667, 9 November 1988.

- [15] W. J. Torné Sandolval, *Fabricación y Caracterización de Películas de Dióxido de Vanadio (VO₂) Depositadas por Sputtering con Corriente Continua Pulsada*, Mayagüez, Puerto Rico, 2011.
- [16] A. Belkind, Z. Zhao, D. Carter, L. Mahoney, G. McDonough, G. Roche, G. Scholl and H. Walde, "Pulsed-DC Reactive Sputtering of Dielectrics: Pulsing Parameter Effects," in *Proceedings of the Annual Technical Conference - Society of Vacuum Coaters*, Denver, 2000.
- [17] APD Cryogenics Inc, Cryopump Model APD-8SC Technical Manual, Revision E ed., Allentown, PA: APD Cryogenics, 1995, pp. 7-8.
- [18] Angstrom Sciences, Angstrom Sciences Onyx-2™ Magnetron Sputtering Cathode - Procedures of Operation, Duquesne, Pennsylvania: Angstrom Sciences, 2006, p. 2.
- [19] J. Y. Suh, R. López, L. C. Feldman and R. F. Haglund Jr, "Semiconductor to metal phase transition in the nucleation and growth of VO₂ nanoparticles and thin films," *Journal of Applied Physics*, vol. 96, no. 2, pp. 1209-1213.
- [20] JCPDS - International Centre for Diffraction Data, *PDF 82-0661*, 2001.
- [21] I. Horcas, F. R, J. M. Gómez-Rodríguez, J. Colchero, J. Gómez-Herrero and A. M. Baro, "WSXM: A software for scanning probe microscopy and a tool for nanotechnology," *Review of Scientific Instruments*, vol. 78, no. 1, 2007.

Appendix A Additional Data

A.1 Transmittance Laser Calibration

		Amplifier (dB)							
		0	10	20	30	40	50	60	70
Melles Griot Laser Intensity (I_o)	5.0	0.0270	0.0460	0.0790	0.1970	0.5720	2.2360	6.8900	10.8700
	5.5	0.0370	0.0780	0.1990	0.5300	1.7830	5.1100	10.8900	
	6.0	0.0470	0.1120	0.3050	0.9170	2.8540	9.0200		
	6.5	0.0580	0.1450	0.4110	1.2530	3.9220	10.8900		
	7.0	0.0690	0.1780	0.5200	1.5980	5.0090			
	7.5	0.0790	0.2120	0.6260	1.9370	6.0860			
	8.0	0.0900	0.2460	0.7350	2.2810	7.1800			
	8.5	0.1010	0.2800	0.8430	2.6690	8.2600			
	9.0	0.1110	0.3130	0.9480	2.9630	9.3200			
	9.5	0.1230	0.3510	1.0560	3.3520	10.4700			
	10.0	0.1340	0.3840	1.1580	3.6780	10.9000			
	10.5	0.1440	0.4160	1.2770	3.9860				
	11.0	0.1540	0.4490	1.3790	4.3130				
	11.5	0.1650	0.4800	1.4760	4.6120				
	12.0	0.1740	0.5170	1.5770	4.9360				
12.5	0.1850	0.5440	1.6880	5.2040					
13.0	0.1960	0.5720	1.7710	5.5330					
		Thor Labs Amplifier Voltage Output (V)							
								Max output limit	

Table 5.1 IR Transmittance characterization laser calibration.

A.2 LabVIEW Measurement File

LabVIEW Measurement

Writer_Version 0.92

Reader_Version 1

Separator Tab

Multi_Headings No

X_Columns No

Time_Pref Absolute

Operator Admin

Description Temperature (K) vs Transmittance (%) and Resistance (Ohm) curves. Measurements made with Keithley 2182 nanovoltmeter, Keithley 2400 Sourcemeter and MMR Technologies K20 temperature controller. Program written by Juan A. Santiago Santos.

Date 9/4/2014

Time 21:05.6

End_of_Header

Channels 3

Samples 1 1 1

Date 9/4/2014 9/4/2014 9/4/2014

Time 21:05.7 21:05.7 21:05.7

X_Dimension Time Time Time

X0 0.00E+00 0.00E+00 0.00E+00

Delta_X 1 1 1

End_of_Header

X_Value

Comment

299	21.900909	98958.14
301.005	21.885076	95038.5525
303.005	21.914605	91335.4675
305.005	21.972471	87824.2775
307.01	22.036948	84447.82
309.01	22.159731	81210.04
311.005	22.261322	78179.1025

313.01	22.364099	75241.7325
314.96	22.471966	72723.5925
317	22.575993	69734.255
319	22.655322	67136.2
320.995	22.69646	64690.4925
323	22.705873	62332.94
325.005	22.660935	60042.69
327	22.607108	57840.5925
329.005	22.479534	55698.855
331	22.298295	53563.8775
333.01	22.080908	51607.4575
335	21.794344	49393.255
336.99	21.511574	47275.0325
338.985	21.248746	45127.87
340.99	20.958665	42527.025
343.025	20.663735	39757.865
345.035	20.25133	35832.97
347.035	19.501623	29609.945
348.95	17.690469	21556.6275
351.01	13.432057	15519.6275
352.975	9.373263	12467.03
355.005	8.20258	11044.995
357.01	7.879463	10321.76
359.01	7.781085	9863.28
361	7.78101	9485.39225
363.01	7.815226	9190.62275
365	7.859369	8927.955
367.01	7.91309	8695.3665
369.005	7.974469	8476.4285
371	8.025712	8265.87725
368	7.928821	8578.869
366	7.852028	8791.6355
364	7.776693	9009.847
362	7.68191	9257.19825
359.995	7.575507	9505.589
358	7.469634	9756.19225
355.995	7.379364	10015.8975

354	7.318056	10311.455
352	7.282085	10618.0175
350.005	7.272916	10944.4625
347.995	7.309282	11337.7175
345.995	7.446167	11826.945
344	7.926798	12604.065
342	10.122602	14406.895
340.01	14.740171	19224
338	17.973287	28787.6575
336	19.72003	37389.0325
334	20.713547	43313.4325
331.99	21.319814	47754.8225
330	21.722133	51185.315
328.01	21.998845	54409.8625
326.01	22.194507	57086.715
324	22.334264	59810.17
322	22.421494	62579.505
320.005	22.447588	65280.7175
318	22.409518	67925.87
316.01	22.31737	70748.3775
314.005	22.190026	73486.9325
312.01	22.054836	76652.3825
310	21.946553	79791.9225
308	21.875846	82957.46
306.065	21.838166	86355.8525
304.085	21.815894	89967.7225
302	21.822829	93448.54
300.005	21.878201	97564.9025
298.5	21.967228	100680.075
297.85	22.016358	102327.85

Table 5.2 File created by the LabVIEW software. Column order: Temperature (K), IR transmittance (%) and Resistance (Ohm)